Investigation of the Temperature-Dependent Mechanical Properties and Deformation Behaviour of Copper-Silver Core-Shell Nanowire: A Molecular Dynamics Study

4 authors, including:

Investigation of the Temperature-Dependent Mechanical Properties and Deformation Behaviour of Copper-Silver Core-Shell Nanowire: A Molecular Dynamics Study

Gourav Kumar Dewangan

Undergraduate Student [18120032], Department of Metallurgical and Materials Engineering, National Institute of Technology Raipur, Great Eastern Rd, Amanaka, Raipur, Chhattisgarh, India, Pin-492010.

K Adityaraj Chowhan

Undergraduate Student [18120035], Department of Metallurgical and Materials Engineering, National Institute of Technology Raipur, Great Eastern Rd, Amanaka, Raipur, Chhattisgarh, India, Pin-492010.

Sumantra Das

Undergraduate Student [18120076], Department of Metallurgical and Materials Engineering, National Institute of Technology Raipur, Great Eastern Rd, Amanaka, Raipur, Chhattisgarh, India, Pin-492010

V. Nandagopal

Undergraduate Student [18120080], Department of Metallurgical and Materials Engineering, National Institute of Technology Raipur, Great Eastern Rd, Amanaka, Raipur, Chhattisgarh, India, Pin-492010.

Advisor: Dr. Subhas Ganguly

Assistant Professor, Department of Metallurgical and Materials Engineering, National Institute of Technology Raipur, Great Eastern Rd, Amanaka, Raipur, Chhattisgarh, India, Pin-492010.

Certificate of Approval

This is to certify that the project entitled "**Investigation of the Temperature-Dependent Mechanical Properties and Deformation Behaviour of Copper-Silver Core-Shell Nanowire: A Molecular Dynamics Study**" submitted by *Gourav Kumar Dewangan (18120032)*, *K Adityaraj Chowhan (18120035)*, *Sumatra Das (18120076)* and *V. Nandagopal (18120080)* to the Department of Metallurgical and Materials Engineering, National Institute of Technology Raipur, for the fulfilment of the requirements for the award of Bachelor of Technology in Metallurgical Engineering has been accepted and that the students have successfully defended the project in the viva voce examination.

(**Dr. Subhas Ganguly**)
Department of Metallurgical and Materials Engineering,
National Institute of Technology Raipur,
Raipur, Chhattisgarh,
India

Declaration

This project work is a presentation of our original research work. Wherever contributions of others are involved, every effort is made to indicate this clearly, with due reference to the literature and acknowledgement of collaborative support and discussion for this work.

The work had been done under the guidance of Dr. Subhas Ganguly, Department of Metallurgical Engineering, National Institute of Technology, Raipur. The result embodied in this report, in full or in parts, has not been submitted by him, elsewhere for the award of any degree or diploma.
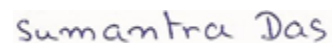
In my capacity as a supervisor of this project work, I certify that the above statements are true to the best of my knowledge.
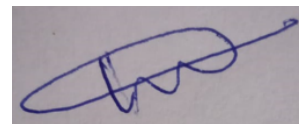
Gourav Kumar Dewangan (18120032)

K Adityaraj Chowhan (18120035)

Sumatra Das (18120076)

V. Nandagopal (18120080)

(**Dr. Subhas Ganguly**)
Department of Metallurgical and Materials Engineering,
National Institute of Technology Raipur,
Raipur, Chhattisgarh

Acknowledgement

Content

Abstract

Copper-silver core-shell nanowires have drawn much attention among researchers due to their exceptional mechanical and thermal properties, combined with excellent conductivity and resistance to oxidation. Thus, they have found a wide range of applications in the field of printed electronics, strain sensors, flexible electronics, interconnects, electrodes, etc. In the present study, Molecular Dynamics (MD) simulation technique was used to investigate the effect of temperature on the mechanical properties and deformation behaviour of a single crystalline copper-silver core-shell nanowire during tensile testing. The mechanical properties like yield strength, ultimate tensile strength and Young's modulus were calculated from the engineering stress-strain curves at different temperatures, in the range of 10-500 K. The variation of Wigner-Seitz defects, dislocations and stacking faults with temperature were analysed and their effects on the mechanical properties and the subsequent deformation behaviour of the Cu-Ag core-shell nanowire were also investigated. The Cu-Ag core-shell nanowire exhibited excellent mechanical properties over the investigated temperature range, with optimum properties at the temperature of 300 K. Moreover, a ductile to brittle transition in the mode of fracture of the Cu-Ag core-shell nanowire was observed below the ultralow temperature of 30 K.

Keywords: *Core-shell*; *Nanowire*; *Copper-Silver*; *Mechanical properties*; *Defects*; *Molecular dynamics*

Introduction

Background

Nanomaterials have gained prominence as a fascinating class of materials in high demand for various applications. The length of a nanometer, a term coined by Richard Adolf Zsigmondy in 1914[1], can be illustrated by lining up five silicon atoms or ten hydrogen atoms. Nanomaterials are defined as having a size or one of their dimensions in the range of 1 to 100 nm[2].

In his speech titled "There's Plenty of Room at the Bottom" at the American Physical Society's annual meeting in 1959, American physicist and Nobel Prize laureate Richard Feynman presented his vision of nanotechnology by posing the question "Why can't write the entire 24 volumes of the Encyclopaedia Britannica on the head of a pin?"[3]. This is believed to be the first academic discussion in this field, where he encouraged the scientific world to develop molecular dimension machines. This speech made him the "Father of Modern Nanotechnology"[4]. In 1974, while stating the phrase "nano-technology mainly consists of the processing of, separation, consolidation, and deformation of materials by one atom or one molecule.", Norio Taniguchi became the first person to scientifically explain the term "nanotechnology"[5].

The emergence of different spectroscopic techniques has accelerated research and development in this domain. In 1982, researchers at IBM developed Scanning Tunnelling Microscopy (STM), which allowed them to procure images of single atoms on "flat" non-tip surfaces[6]. In 1986, Atomic Force Microscopy (AFM) was devised and has since evolved into the most important scanning probe microscope technique[7]. The desire to create high-density hard discs prompted the evaluation of magnetic and electrostatic forces, which encouraged the development of Kelvin-probe, magnetic-force and electrostatic microscopy[8]. Nanotechnology is constantly advancing and is now an omnipresent materials chemistry.

Another important area that further developed nanotechnology is the field of computational material science and engineering, particularly the Monte Carlo technique, Molecular Dynamics and Density Functional Theory. With the success of the Monte Carlo Method, the scientific community started to work on solving multibody problems computationally. This led to the development of several Molecular Dynamics methods, including Verlet's algorithm[9]. In an attempt to understand the basis of irreversibility, Fermi computed to estimate the evolution of time in the equations of motions under different laws of force for a multi-body system

using MANIAC I, which was published in 1953 and popularly known as the seminal work of Fermi−Pasta−Ulam−Tsingou problem[10]. The radiation damage simulation of solid copper (Cu) by Gibson et al. in 1960 using a Born−Mayer type of repulsive interaction along with a cohesive surface force was the first realistic simulation[11]. The highly accurate data obtained by Rahman in 1964 from the simulations of Lennard-Jones potential based liquid argon while compared with experimental data proved the validity of the method[12].

Nanotechnology is a perfect representation of emerging technology, as it provides engineered nanomaterials showing significantly improved performance compared to traditional materials. Nanomaterials have found profound applications in electronics, surface coatings, environmental remediation, sensors, and energy-storage devices.[13]

Problem Statement

With the advent of nanotechnology, the scientific community has been actively engaged to explore this field. Nanowire is one such nanomaterial that has intrigued the scientific world. It is defined as the one-dimensional (1-D) nanostructures having nano-order diameter, and aspect ratio of 1000 and more. These 1-D nanomaterials show several interesting features which are not observed in 3-D bulk materials. One such property is the dominance of quantum mechanical effect due to its lateral quantum confinement of electrons leading to energy level occupation distinct from those observed in bulk materials. This encouraged the scientific world to call these nanowires quantum wires.[14]

Some nanowires show discrete values of the electrical conductance due to the quantum mechanical restraint on the electron counts in the conductance band in the nanoscale width wire[14]. This quantum of conductance is described by the following equation:

$$\frac{2e^2}{h} = \frac{2}{R_K} \simeq 77.41 \mu S \tag{1}$$

where R_K refers to the von Klitzing constant and is approximately measured to be 25812.8 Ω. The fixed conventional value R_{K-90}[15] is considered to be the standard since 1990.

In recent times, nanowires found profound applications in nanoelectromechanical, optoelectronic and electronic devices, metallic interconnects in nano-quantum devices, additives in advanced composites and leads in biomolecular nanosensors.[16]

There are various forms of nanowires as described, but core-shell nanowires have recently intrigued the scientific community. In this study, a molecular dynamic analysis of mechanical properties of Cu-Ag core-shell nanowire is investigated. The Cu wires have been extremely beneficial in electrical applications, but with the increase in demand for nanoscale devices, there was a need for an electronic nanowire that has high conductance and efficiency yet is economically viable. The Cu nanowires have been fruitful to serve such a purpose[17]. However, their susceptibility to corrosion under normal atmospheric conditions and early failures of nanodevices encouraged the synthesis of the Cu-Ag core-shell nanowire, where the Cu core is protected by the silver (Ag) shell that surrounds it[18]. The synthesis of such material for testing is quite expensive and hence a molecular dynamic approach is considered for the present study to investigate the mechanical properties and the deformation behaviours of the Cu-Ag core-shell nanowire under different temperatures.

Objectives of the Research

In this study, the primary objective is to understand the mechanical properties and the deformation behaviours of the Cu-Ag core-shell nanowire under different temperatures. Initially, a critical literature review on nanomaterials, particularly the mechanical properties and deformation behaviour of nanowires, is conducted to familiarise with the concerned problem statement. Based on the understanding, an MD programme for tensile testing of copper-silver (Cu-Ag) core-shell nanowire of a fixed configuration under different temperatures, namely 10K, 100K, 200K, 300K, 400K and 500K were developed. The results yielded, particularly vacancy defects, dislocations, stacking faults, modulus of elasticity, ultimate tensile strength and yield strength, were then analysed using OVITO.

Scope

This study may help in the following manner:
- Proper theoretical understanding of the mechanisms involved in the mechanical behaviours of the nanowire with respect to temperature is possible.
- It shall serve as the guiding manual for developing a new generation of nanowires where temperature plays a critical role in mechanical properties and structural applications.

Thus, the study shall pave the path for further investigations which will benefit the experimentalists to design the optimised nanowire configurations for concerning applications with varying temperatures.

Literature Review

Information

Ye et al. (2014) investigated the high aspect ratio copper nanowire (Cu NWs) produced faster by the ethylenediamine (EDA) based Cu(II) reduction that is conducted at atmospheric pressure. They realised that the N_2H_4 concentration of less than 5.7 mM prevents the radial growth, while an EDA concentration of less than 95 mM prevents the tapered growth but higher concentrations reduce the axial growth rate. This was the first communication to report the synthesis of Cu NW with an aspect ratio of 5700, the highest one to date with solution coating, in 30 minutes that is utilised in designing transparent conductance film with transmittance of more than 95% and sheet resistance less than 100 Ω/sq.[19]

The paper of Wei et al. (2015) was the first to report the application of Cu-Ag core-shell nanowire in the electronic skin with petal moulded microstructure. The electronic devices, biomedicine, robotic system etc. can be developed by multiple folds with the introduction of flexible electronic skin (e-skin) that could be cost-effective with the implementation of highly conductive and flexible Cu NWs as a conductive filler. But the oxygen sensitiveness of Cu NWs discourages the technologists from its development. Wei et al. utilised the superior oxidation-resistant Cu–Ag core-shell nanowires (Cu–Ag NWs) developed from the parent Cu NWs, whose surface was coated by a 20 nm thin Ag using the facile galvanic replacement reaction without undergoing stirring or heating. A bio-inspired piezoresistive e-skin was achieved by replicating the microstructure into a rose-petal based surface and introducing it onto the 2D polydimethylsiloxane (PDMS) to achieve a low detection limit (<2 Pa) and response and relaxation times (36 ms and 30 ms) while maintaining excellent sensitivity (1.35 kPa⁻¹) and working stability (>5000 cycles). Wei et al strongly believe that high-performance e-skin with such filler shall find profound applications in spatial pressure distribution detection, wrist pulse monitoring and voice recognition.[20]

Stewart et al. (2015) reported the synthesis of copper-platinum (Cu-Pt), copper-gold (Cu-Au), and Cu-Ag core-shell nanowires (NWs) through a room-temperature solution-phase process. The products yielded are subjected to ascorbic acid for the galvanic replacement prevention, the noble metal ions reduced onto the Cu NWs and the passivating copper oxide coating removal from the same. While the report cites the superiority of the printed Cu-Ag NWs over conventional Cu NWs through its electrical conductance in any condition and oxidation resistance in humid conditions

(85% RH) at 85°C and dry air at 160 °C for 24 hours, such Cu-Ag core-shell NWs based films are also reported to be superior over Ag ones in terms of optoelectronic properties under same aspect ratio.[21]

Wang and Shin (2017) investigated the nanojoining processes of Ag nanoparticles (NPs), Cu-Ag core-shell NPs and nanowires (NWs) that have found profound applications in microelectronic industries, particularly room temperature T_{room}=300K through molecular dynamics simulations in order to design nano-joint with necessary mechanical, electrical and thermal properties. The three-stage nanojoining mechanisms that involve crystallisation-amorphisation, reorientation and Shockley partial dislocation, are determined and influenced by densification, potential energy and structural deformation. In comparison to pure Ag nanomaterial, The higher densification and room temperature bonding strength of Cu-Ag core-shell nanomaterial is influenced by the Cu core without the joining process but improves the Ag shell mobility.[22]

Ma et al. (2017) presented the variations of microstructures and the mechanical properties of Ni-200 samples brazed by Cu-Ag core-shell nanowire nanopastes and Ag nanopastes under the brazing temperature and pressure. The improvement of shear strength was observed with the enhancement of the brazing temperature from 300 °C to 850 °C and brazing pressure from 7 MPa to 26 MPa due to the promotion of the diffusions between adjacent nanoparticles and nanowires, and hence between the seam and base materials. This study indicates that a superior brazed sample with 40.6 MPa is prepared at the brazing temperature of 700°C, suggesting the nickel brazed by Ag nanopastes can be prepared at a brazing temperature lower than those by the commercially viable BAg-8 brazing filler metals.[23]

Sarkar et al. (J Nanopart Res., 20 (1), 2018) reported a molecular dynamics-based study on Cu−Ag core-shell nanowires with diameters of 9-30 nm and varying core diameter, shell thickness, and strain velocity to investigate tensile properties such as yield strength, ultimate tensile strength, and Young's modulus. The conclusions drawn from the extrapolation of various strain velocities on a predefined wire size were used to measure tensile properties such as yield strength and Young's modulus at a standard strain rate of 1 mm/min. These findings demonstrate the superiority of ultra-high tensile properties of Cu−Ag core-shell nanowires over bulk Cu and Ag and suggest they be used as reinforcing agents in ultra-high strength nanocomposites.[24]

Sarkar et al. (J Nanopart Res., 20 (10), 2018) investigated the deformation mechanism of Cu-Ag core-shell nanowire during tensile testing with varying temperatures through a Molecular Dynamics study to understand the factors responsible for their mechanical properties. During deformation, while the total number of vacancies and interstitials were analysed by the Wigner-Seitz defect analysis, the type, number, and

total length of dislocation segments were analysed by the Dislocation extraction algorithm (DXA). The authors also investigated the influence of core diameter and shell thickness on these properties.[25]

Cruz et al. (2018) reported the synthesis of 4.4g Cu nanowire with a diameter of 240 nm in 1 hour and the 3 nm oxidation-resistant Ag coating such that Ag:Cu mol ratio of 0.04 over the same in 1 hour, marking the first such conductive polymer composite filament for 3D printing with resistivity as low as 0.002 Ω.cm, more efficient than graphene-based 3D printing filaments in terms of conductivity. The paper cites the synthesis of highly conductive composites with relatively low volume fractions, 3D printed conductive coil that could enhance the wireless power transfer, based high-aspect ratio of Cu-Ag nanowires after indicating the greater conductivity of composites containing 5 vol% of 50 µm long Cu-Ag nanowires compared to that containing 22 vol% of 20 µm long Ag nanowires, and the current density between 2.5 and 4.5×10^5 A.m^{-2} is controlled by the surface-to-volume ratio.[26]

Weng et al. (2018) realised that the lattice-mismatch is responsible for the formation of polycrystalline shell layer and the creation of a non-coherent interface, thus influencing the heteroepitaxial growth of core-shell nanostructures. The paper reports the synthesis of dense twin boundaries based Cu-Ag core-shell nanowire through the galvanic replacement reaction, such that the nanotwinned Cu nanowire is grown epitaxially with its twinning structure replicated by the Ag shell due to the large lattice mismatch between Ag and Cu (~12.6%). The paper highlights the twin-mediated epitaxial growth mechanism which involves the coherent twin boundaries that influences the misfit dislocations in the high lattice-mismatch bimetallic systems.[27]

Believed to be the alternative to indium tin oxide, Zhang et al. (2019) synthesised the highly stable Cu-Ag core-shell nanowire through the two-step adsorption and decomposition method that could be an improvement over the traditional cost-effective, conductive, transparent but oxidation-prone Cu nanowire. The Cu_2Ag-amine complex is first formed on the Cu nanowire surface through the Ag-amine complex adsorption, and then Ag shell thickness, responsible for restricting the Cu nanowire oxidation, is controlled by silver-amine solution concentration. The Cu-Ag core-shell nanowires so produced have similar properties as that of Cu nanowires, i.e. high conductivity and transparency.[28]

Sarkar et al. (2022) investigated the thermal properties, including thermal conductivity, melting point, specific heat capacity, and coefficients of thermal expansion, of Cu-Ag core-shell nanowires with respect to the dimension using a non-equilibrium molecular dynamics simulation. The authors have observed the lowering of thermal conductivity with respect to the bulk Cu, and also distinct

features, like the negative thermal expansion coefficients and the melting point of 1369.8 K.[29]

Literature Summary

The synthesis of different forms of nanomaterials, namely nanoparticles and nanowires, has revolutionised different sectors, particularly electronic industries, to a great extent. The commercially cheaper[28], transparent[28], highly conductive[28] and flexible[20] Cu nanowires are vulnerable to oxidative degradation[25], which is overcome by the development of oxidation-resistant[18] Cu-Ag nanowires with all requisite properties of Cu nanowires and Ag nanowires that are described to be synthesised by different methods namely ethylenediamine (EDA) based Cu(II) reduction[19] and two-steps adsorption (through Cu_2Ag-amine complex formation) and decomposition method (controlling silver-amine complex for Ag shell)[28]. The bio-inspired piezoresistive thin film of superior oxidation-resistant Cu-Ag core-shell nanowires for electronic skin is synthesised, followed by the 2D polydimethylsiloxane for rose-petal mould microstructure to attain detection limit <2 Pa, response and relaxation times 36 ms and 30 ms respectively, the sensitivity of 1.35 kPa^{-1} and working stability of more than 5000 cycles[20].

A superior brazed sample with 40.6 MPa is prepared at the brazing temperature of 700°C, lower than those by the commercially viable BAg-8 brazing filler metals, by Ag nanopastes.[23] The core-shell nanostructures with polycrystalline shell layer is grown hetero-epitaxially influenced by the misfit dislocations in the high lattice-mismatched bimetallic systems.[27]

The Molecular Dynamics studies on different core diameters, shell thicknesses and strain velocities on the tensile properties of Cu–Ag core-shell nanowire reveal the superiority of ultra-high tensile properties of Cu−Ag core-shell nanowires over bulk Cu and Ag nanowires, which suggests its use as a reinforcing agent in ultra-high strength nanocomposites.[24] While the Molecular Dynamics studies on the deformation mechanism during tensile testing of such nanowire with the varying core diameter and shell thickness reveal the distribution behaviour of vacancies and interstitials by the Wigner–Seitz defect analysis and the types, counts and lengths of dislocations by the DXA in OVITO[25], those on thermal properties, including thermal conductivity, melting point, specific heat capacity, and coefficients of thermal expansion indicates the features like lowering of thermal conductivity with respect to the bulk Cu, a high melting point of 1369.8 K and negative thermal expansion coefficient[29]. Further, the Molecular Dynamic investigations of the mechanism of nanojoining of Ag nanoparticles, Cu-Ag core-shell nanoparticles and nanowires,

involving crystallisation–amorphization, reorientation and Shockley partial dislocation, to design nano-joint with necessary mechanical, electrical and thermal properties[22].

Mechanical Aspects of Nanowire

Mechanical properties

The emergence of the Atomic Force Microscope (AFM) and accompanying technologies, which allowed direct observation of nanowires, has boosted the research on nanowires.[30] An AFM tip can restrict a nanowire on one side while moving the unrestricted side. The height and the exerted force of the AFM comprise this cantilever configuration, which translates the nanowire's parameters into a stress vs. strain curve.

Young's modulus of nanowires

The Young's Modulus, which serves as a reliant characteristic of nanowires, is used to determine the elastic portion of the stress-strain curve for nanowire. The modulus-diameter relationship could be estimated using continuum mechanics:

$$E = E_0\left[1 + 4\left(\frac{E_0}{E_s - 1}\right)\left(\frac{r_s}{D} - \frac{r_s^2}{D^2}\right)\right] \tag{2}$$

Where the symbol E_s denotes surface modulus, r_s denotes shell thickness, E_0 denotes bulk modulus and D denotes the diameter of the nanowire under tension.[30]

Though the equation suggests that modulus increases as the diameter shrinks, Molecular dynamics and other computational methods indicate that modulus is directly proportional to the diameter of the nanowire.

Nanowire yield strength

The yield strength of the nanowire, marked by the onset of plasticity, is an indication that the strength is enhanced by minimising its flaws. The increment of strength to the molecular tensile strength should theoretically rise with the shortening of a horizontal array of particles[30]. The 'dislocation-starvation' mechanism, which states that the nanowire is subjected to enormous strains before the dislocation motion is conceived and strain hardening is experienced, is in action when there is no or less dislocation or its associated motion. The ongoing research on nanowires is focused to improve the mechanical properties for MEMS or NEMS devices.

Nanowire ultimate tensile strength

The ultimate tensile strength of the nanowire, marked by the onset of necking in ductile fracture, is an indication of the maximum stress the nanowire can withstand before undergoing fracture. This is an important parameter to consider in structural applications. It is observed that the brittle failure is experienced at an extremely low temperature, while ductile failure is observed at a higher temperature.[31]

The brittle failure has been one of the primary concerns for the material scientists as they fail without providing any signal. However, in cases of FCC based nanowires, they occur at temperatures below the Ductile-to-Brittle Transition temperature.[31] This failure undergoes three stages[31]:
- The dislocation pile-ups along the slip planes serve as the obstacle to plastic deformation.
- The microcracks are nucleated at the head of these pile-ups, where the shear stresses are built.
- The microcracks are further driven to fracture without dislocation movements due to the stored strain energy.

The ductile failure, on other hand, often provides a signal through elongation or necking. This failure generally takes place at a higher temperature, especially temperature above Ductile-to-Brittle Transition temperature.[31] Such failure, popularly called rupture, follows the ductile "cup-and-cone" fracture, and undergoes the below-mentioned stages in a sequential manner[31]:

- The point of plastic instability, characterised by necking, experiences a failure of compensation between the rise in strength due to strain hardening and the fall in the cross-sectional area.
- Several fine cavities are formed in the region.
- These cavities grow and coalesce as a central crack due to continuous straining.
- This crack grows towards the surface in a direction perpendicular to the axis, before propagating along a localised shear plane roughly 45° to the axis for the formation of a "cone".

Thus, it is important to determine the ductile-to-brittle transition temperature in order to identify the probable mode of fracture during the operation.[31]

Defects in nanowires

The perfect crystals are the ideal crystals that are possible to acquire in extremely low temperatures where the entropy is zero. The third law of thermodynamics dictates

that the entropy of a perfect crystal is zero at the temperature of absolute zero[31]. The deviations from the orderly lattice points' arrangement in zero to three-dimension, known as defects or imperfections, are inevitable features in a crystal at non-absolute temperatures[32].

Vacancies

The zero dimension defects of vacancies are the ones where the atoms go missing from the lattice sites. These are thermal defects formed during solidification due to vibration and local rearrangement of atoms, plastic deformation and ionic bombardments.[32] They are mainly found in the bulk while being absent in the nanostructures.

$$\frac{n}{N} = exp\left(-\frac{E_s}{kT}\right) \qquad (3)$$

where n and N represent the number of vacancies and atoms, E_s represents the activation energy, k represents the Boltzmann constant and T represents temperature.[32]

Dislocations

The one-dimensional defects of dislocations are responsible for the slip phenomena that allow the metal to deform plastically.[32]

In Face-Centred Cubic structure, 1/2<110> and <001> serve as the shortest lattice vectors, probably Burgers vectors, for dislocations. However, the perfect dislocation is the one whose glide away from the plane leads to the formation of a perfect crystal lattice. Therefore, 1/2<110> rightly serves as perfect dislocation in FCC structure.[33]

When the perfect dislocation dissociates into a pair of partial dislocations that are glissile in nature and lie in the plane of fault, this is called the Shockley partials. These partials are responsible for the formation of the stacking fault.[33]

$$\frac{a}{2}[10\bar{1}] \rightarrow \frac{a}{6}[2\bar{1}\bar{1}] + \frac{a}{6}[\bar{1}\bar{1}2] \qquad (4)$$

Similarly, other partials which are generated from the perfect dislocations are the Frank partials. These are sessile in nature, but can move through diffusion[33]. It is represented by the following Burger's vector:

$$b = \frac{a}{3}[111] \qquad (5)$$

It is already well established that two perfect dislocations on different {111} planes dissociate into Shockley partials. These Shockley partials move and associate to form a stair-rod dislocation with a sessile Lomer Cortell dislocation at the tip.[33]

$$\frac{a}{6}[\bar{1}2\bar{1}] + \frac{a}{6}[1\bar{1}2] \rightarrow \frac{a}{6}[011] \tag{6}$$

The interactions between abundant sessile dislocations of different glide planes may either lead to dislocation annihilation or cause dislocation locks, especially the ones that are not in the slip directions. These locks, which form stable dislocation segments in crystallographic directions of [100], form Hirth dislocations and serve as barriers to mobile dislocations in the concerned slip system.[34]

Stacking Faults

The continuous repeating pattern of crystals may sometimes be interrupted due to the presence of other defects, namely vacancies and the Shockley partial dislocations[34, 35]. These two-dimensional planar defects in crystalline materials are stacking faults, which often arise during plastic deformation and crystal growth[32, 36]. It is noteworthy to state that the low stacking-fault energy results in a stacking fault bounded by partial dislocations[37]. It is also important to cite that the agglomeration of vacancies leads to intrinsic stacking fault, while those of interstitials lead to extrinsic stacking fault[37].

Methodology

Introduction to Molecular Dynamics

Molecular Dynamics (MD) is the subfield of computational material science, which is based on classical mechanics principles and involves the study of modelling the time-dependent behaviour of a particle system that incorporates Newton's equations of motion among the interacting atoms confined within properly described boundary conditions. This method reveals information about atomic locations and velocities at the microscopic level with proper interaction potential as an input. Statistical mechanics is used to changing this microscopic information into macroscopic measurements such as pressure, temperature and stress tensor. Computer simulations were used in the hopes of better understanding the characteristics of molecular assemblies in terms of structure and microscopic interactions.[38]

Computer simulations not only help to understand the structural and the interactional characteristics of molecular assemblies but also act as a link between microscopic length and time scales in the macroscopic world. The complexity of determining the parameters associated with such large molecular systems is solved by MD simulation through numerical approaches.[38]

Two essential components of MD include[38]

- Interatomic potential values for calculating forces between atoms and molecules.
- Equations that determine the position and motions of particles at any time.

Classical mechanics, as derived from Newton's equations, show that the force F_i exerted on i^{th} atom possessing mass m_i, acceleration a_i and position r_i is equal to the negative value of the potential energy (V) gradient associated with the position of the particle. It is also important to state that the systems considered for MD simulations are always subjected to the conservation of Hamiltonian. Hence it is a deterministic approach.[38]

$$F_i = m_i a_i = m_i \left(\frac{d^2 r_i}{dt^2} \right) = \nabla_i V = \left(\frac{dE}{dr_i} \right) \qquad (7)$$

The above equations, if solved, reveal acceleration a_i, velocity v_i and position r_i of the ith atom.[38]

$$a_i = \left(\frac{dv_i}{dt} \right) \tag{8}$$

$$v_i = \left(\frac{dr_i}{dt} \right) \tag{9}$$

The Verlet algorithm in MD simulation is referred to as a second-order integrator, because of the significantly larger global error compared to local ones in MD simulation. Based on the previous position data from time t and t-δt, the position of the atom r(t-δt), with local error and global error lie in $O(\delta t^4)$ and $O(\delta t^2)$ respectively, can be predicted by the following equation:[38]

$$r(t + \delta t) = 2r(t) - r(t - \delta t) + a(t)\delta t^2 + O\left(\delta t^4\right) \tag{10}$$

The velocity determined from equation (11) possesses the local and global error of $O(\delta t^2)$.[38]

$$v(t) = \frac{r(t + \delta t) - r(t - \delta t)}{2\delta t} \tag{11}$$

LAMMPS and its implementation

Large-scale Atomic/Molecular Massively Parallel Simulator (LAMMPS), a free and open-source molecular dynamics simulation software developed by Sandia National Laboratories as part of a Cooperative Research and Development Agreement (CRADA) with two laboratories from the US Department of Energy and three additional laboratories from private sector companies, uses the Message Passing Interface (MPI) for parallel communication and is trademarked under the GNU General Public License.[39]

It is a classical MD programme that simulates atomic, polymeric, biological, solid-state (metals, ceramics, oxides), granular, coarse-grained, or macroscopic systems with particle ensembles in liquid, solid, or gaseous states using various interatomic potentials and boundary conditions. LAMMPS also includes support for OpenMP multi-threading, vectorization, and GPU acceleration. It integrates Newton's equations of motion for a number of interacting particles. Its interaction models are generally short-range in nature, while several long-range models are given as well. The software employs neighbour lists to track adjacent particles.[39]

Steps to simulate the nanowires in LAMMPS

The designed nanowire is simulated using LAMMPS in the following steps:

- Using LAMMPS, the mechanical properties of Cu-Ag Core-Shell Nanowire are simulated and analysed.
- In LAMMPS, the Cu-Ag Core-Shell Nanowire with a core diameter of 20 $\mathring{A}$ and shell thickness of 5 $\mathring{A}$ and length of 200 $\mathring{A}$ is designed with known parameters.
- The periodic conditions in all the 3 dimensions are chosen as the boundary conditions and the time-step of 1 fs is considered for the study.
- After creating the nanowire, the three regions, i.e. Upper Grip region, Lower Grip region and the middle interacting Gage region are defined.
- The whole system is equilibrated using an NPT ensemble at 300.0 K and pressure of 0.0 bars in all 3 dimensions for around 50,000 time steps.
- After this step, the tensile testing is performed on the nanowire sample by giving velocity to the upper region of 2 $\mathring{A}$/ps.
- The force applied on the nanowire is calculated by the force command along the Z-axis. The displacement of the Upper region is computed using the displacement command. The temperature of the middle region is also computed.
- The whole simulation runs for 1,50,000 time-steps until the desired result has not been achieved. The output files are printed both in log and dump files.
- After getting the log file, the plot to calculate the stress vs strain curve, as well as potential energy vs time-step, was obtained. Analysis of the simulation in video format was done using OVITO software.

OVITO and its implementation

OVITO is a scientific data visualisation and analysis programme to extract useful information for various particle-based simulation models often used in computational materials science, physics, and chemistry, which provides a wide range of fundamental viewing and analysis features that may be assembled into a processing sequence. This information includes particle coordinates, types, velocities, energies, crystal structure etc. The programme will then apply these processes based on mathematical formulae, which are all adjustable, to the simulation data in real-time. The customisation option of mathematical formula available to the user encourages one to derive own sets of data that include scalar, vector, or tensor data fields at every particle. The data pipeline's output is displayed on a screen that can be exported as output data files.[40]

The current version of OVITO supports the following tasks[40]:

- Atoms can be coloured according to their kind, selected status, or any other per-atom data in the input file or generated in the pipeline.
- Atomic transformation and the simulation cell.

- Calculation and presentation of displacement vectors caused by differences between two system states.
- Interactive atomic structure slicing and cutting.
- Periodic picture display and atom wrapping at periodic boundaries.
- Atoms are chosen depending on user-defined parameters.
- Atomic bond calculation and visualisation.
- Calculating ambient lighting and colouring atoms for improved viewing of three-dimensional atomic structures.

OVITO can handle multi-time step data files, allowing users to see how the system evolves over time. Every user activity may be undone, and nearly every parameter can be animated, allowing for the creation of fly-through movie animations of the atomic structures. In addition, OVITO may show three-dimensional polygonal data and geometric forms, allowing the user to supplement the atomic data with extra visual assistance.[40]

Steps to observe the simulation in OVITO

Following steps were undertaken to visualise the simulation:

- Using OVITO, the dump file received after the LAMMPS simulation is studied and analysed.
- The initial nanowire structure and its evolution with the advancing time-steps is observed in the OVITO.
- Changes in the three dimensions and the tensile failure towards the end are studied using the OVITO.
- The Wigner-Seitz Defect Analysis helps to analyse the vacancy counts at the end of thermal equilibrium and the changes of the same during straining.
- The Dislocation Analysis feature helps to analyse different dislocation (Perfect, Shockley, Stair-rod, Hirth, Frank) counts at the end of thermal equilibrium and the changes of the same during straining.
- The Structure Analysis of the Dislocation Analysis feature helps to analyse FCC and HCP counts at the end of thermal equilibrium and the changes of the same during straining. When HCP structures are observed in the FCC ones, then they indicate the stacking faults.

Wigner Seitz Defect Analysis

This analysis modifier implements the Wigner-Seitz (WS) cell method to determine the counts and the movements of vacancies and interstitials. The reference configuration, which specifies the number of defects in a perfect crystal, and the displaced configuration, which indicates the locations of such defects, are the two

atomistic methods to implement in this analysis. The distinction of the designation of atoms from the reference configuration as sites and those from the displaced configuration as atoms indicates that the atoms in the reference configuration specifies only the expected ones in the expected position while those in the displaced configuration specifies real atoms. The analysis confirms the occupation of a site by an atom if it is present on or near the site. Finally, each atom would be allocated to a specific site. However, there remain minor anomalies in every case. While the sites with no occupation of atoms are referred to as vacancies, the sites with the occupation of multiple atoms are referred to as interstitials. The Wigner–Seitz cell, or Voronoi cell, is mathematically described as the locus of points in space closer to the concerned atomic sites while considering the reference configuration.[40]

It is adequate to predict the nearest site to decide the cell of the concerned atom without constructing geometric shapes of WS cells. It reduces the algorithm to a point-to-point search that determines the closest site and adds one to the site's counter, which is defined as an occupancy number. When the number of vacancies and those of interstitials is equal, the algorithm identifies that the number of atoms in the displaced configuration and those in the reference configuration is equal. This is attributed to the fact that the sum of all occupancy numbers equals the number of sites in the reference configuration.[40]

Steps to identify the number of vacancies at the end of equilibrium:

- "Wigner–Seitz Defect Analysis" is first selected from the panel.
- "Atoms (displaced config)" and "Compute per type occupancies" are selected in "Affine mapping of simulation cell".
- "External file" is selected in "Reference configuration source".
- The CFG file (Frame number: 0) of the initial design is opened.
- Frame number: 50 is selected to determine the number of vacancies at the end of equilibration, which is in 5000 steps in this study.

Steps to identify the number of vacancies during straining:

- "Wigner–Seitz Defect Analysis" is first selected from the panel.
- "Atoms (displaced config)" and "Compute per type occupancies" are selected in "Affine mapping of simulation cell".
- "External file" is selected in "Reference configuration source".
- The CFG file (Frame number: 50) of the nanowire, which has already undergone thermal and energy equilibration, is opened.
- Frames from 50 to the point of Ultimate Tensile Strength determined from the stress-strain curve (obtained from the deformation file as developed in the code) are selected to determine the number of vacancies during straining.

Dislocation Analysis

Using the Dislocation Extraction Algorithm, a canonical method of differentiating the dislocation from the crystal and determining the Burgers vector, this analysis modifier identifies and displays all dislocations in the form of lines. For a given Burgers circuit C, the translation of each line element Δx to the corresponding image $\Delta x'$ by the mapping $\Delta x \rightarrow \Delta x'$ indicates[41, 42]:

$$b = -\sum_{C'} \Delta x'$$

The algorithm, supported by Common Neighbor Analysis (CNA) method maps each edge of the Delaunay tessellation, which helps to describe the set of elementary atomic steps, to a corresponding vector of the concerned ideal crystal. Based on the deviation of crystallinity, the algorithm segregates the good regions (where crystallinity is maintained) from the bad ones, and this two-dimensional boundary of separation enclosing the defect in a three-dimensional system is marked as the interface mesh. Thus, the trial circuit is the closed sequences of tessellation edges evaluated by adding all the lattice vectors as mentioned in the equation. The circuit, which has an appearance of a rubber band around dislocation, is prevented from sweeping by imposing a hard limit on the maximum circuit length.[41, 42]

The input parameters for Dislocation analysis are mentioned below[41, 42]:

- Input crystal type: While the DXA can currently identify only 4 crystal structures, namely FCC, BCC, HCP and diamond structure, the rest are defined as "Others".
- Trial Circuit Length: It sets the limit to the maximum length of the trial Burgers circuit. By default, it is 14, which suffices to identify all lattice dislocations along with their types.
- Circuit stretchability: The variation of dislocation core encouraged the development of this feature, which allows the algorithm to extend dislocation in order to mimic the elasticity, set default as 9 for the stretchability parameter.
- Use only selected particles: This feature can identify only the atoms of interest selected by the user when activated while assigning the rest as "Others". It is beneficial in distinguishing crystals possessing a sublattice supported by the program from structures not supported by the modifier.
- Output interface mesh: This is a feature to identify the interface mesh.
- Generate perfect dislocations: This feature helps one to identify only perfect dislocations by disabling partial dislocations, stacking faults and twinning

dislocations, which is only beneficial in certain cases where the information of perfect dislocations alone is important for the study.

- Line smoothing level: This feature helps to post-process the generated raw data of dislocation by smoothing the dislocation curves by controlling the number of iterations in the algorithm.
- Line point separation: This feature smoothens the dislocation lines by reducing the points in the post-processing step.
- Surface smoothing level: This feature smoothens the defect mesh by controlling the number of iterations in the algorithm.

The output parameters for Dislocation analysis are mentioned below[41, 42]:

- Dislocation lines: These are the continuous lines, which possess a starting point and an end point (if remain open) that define their orientation. They may either end as junctions or remain dangling. Sometimes, they form a loop leading to 2 junctions with its end. The Ovito output also reveals the identification of the crystallite structure it is localised and its Burgers vectors.
- Defect mesh: DXA algorithm distinguishes the good region and the bad regions, that are separated by two-dimensional manifolds of the interface mesh. While the good region possesses perfect crystallinity of known (by the program) type, coherent grain boundaries and stacking faults, the bad ones possess unidentified defects, crystal voids and outer surfaces. While the interface mesh encloses the dislocation defects, the defect mesh encloses the triangulated non-dislocation defects that indicate the bad crystal region.
- Atomic structure types: Based on Common Neighbor Analysis, this feature helps to identify atoms that occupy positions of some crystal type known by the Ovito. In FCC, DXA determines the arrangements of FCC and HCP atoms. This HCP arrangement indicates the occurrence of stacking faults and coherent twin boundaries.
- Atomic clusters: After atomic structure types' identification, the cluster of atoms of the same crystal type forms an adjoining crystallite that has been designated by the algorithm a unique ID. While HCP clusters represent stacking faults in FCC crystal, the coherent twin boundary of an FCC bicrystal can be identified by two FCC clusters, indicating grains, and one HCP cluster, indicating boundary cores.

In this work, DXA analysis in Ovito helped to determine the count of various dislocations and stacking faults at the end of equilibration and during straining in different temperatures. As mentioned earlier, the stacking faults can be determined by the number of atoms in the HCP arrangement. The distributions and the stacking faults are also observed visually in the Ovito.[41, 42]

Computational Strategy using LAMMPS

Tensile deformations were simulated in LAMMPS[43], while the data of crystal structures, defects and dislocation were analysed and visualised in OVITO[41]. The Cu-Ag core-shell nanowires of 20 Å core diameter and 5 Å shell thickness were developed in LAMMPS using the built-in crystal structure generation algorithm. The orientation of the nanowires was maintained such that the (001) plane and the [001] direction lies perpendicular and parallel to the cylinder's axis respectively. To compensate for the infinite length circumstance and inhibit lateral deformation, periodic boundary conditions were used throughout the investigation. The atoms were designated an initial velocity based on the Maxwell-Boltzmann energy distribution function, which is mapped to its equilibration temperatures of 10 K, 100 K, 200 K, 300 K, 400 K and 500 K[44]. Then, the nanowires were simulated to thermal equilibration at these temperatures using the canonical NPT ensemble. The interatomic potential, defined by an alloy type "Embedded Atom Method" potential, indicates the precision and the accuracy of simulation results[45]. To investigate the effect of changing the temperature on defect and dislocation behaviours, simulations were run with the temperature being the variable while fixing the initial dimension of the nanowire mentioned earlier and strain rate. To achieve sufficient thermal stability and relaxation of the nanowires, thermal equilibration was performed up to 50 ps, where each time-step is 1 ps. Similar to the practical experiment of tensile testing, the tensile deformation of these nanowires was simulated in the aforementioned equilibrated temperatures. After fixing one-sixth of the nanowires at both ends, the lower end was transfixed while the upper end was pulled along the longitudinal direction at a strain velocity of 2 Å/ps.

OVITO was used for the Wigner-Seitz defect analysis to estimate the vacancies and the interstitials, and the detailed dislocation analysis by implementing DXA at the end of thermal equilibration and changes in each stage of the deformation process. The results, including the Wigner-Seitz defect, the type and the number of the dislocation segments and the stacking faults were plotted to investigate their variation throughout the deformation process, as well as with changes with respect to temperature. For different temperatures, snapshots of dislocation and stacking fault configurations inside the nanowires during deformation were procured by concealing the atoms for clarity of the study. The dislocation behaviours with respect to temperature during the deformation were carefully examined and associated with the mechanism of tensile deformation.[41, 42]

Result and Discussion

A Cu–Ag core–shell nanowire of core diameter of 40 Å, shell thickness of 10 Å and length of 200 Å is modelled in LAMMPS, with its available functions. The design of such a nanowire without thermal equilibrium is presented in Fig. 1.
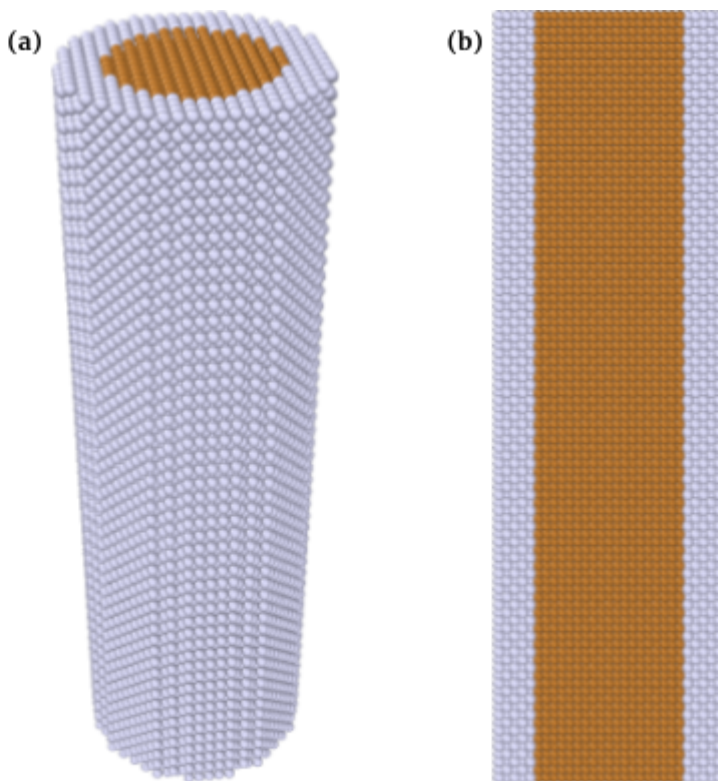

Fig. 1. (a) Isometric projection and **(b)** sliced-section of non-equilibrated perfect crystal of copper–silver core–shell nanowire. Here, brown atoms represent copper ones and grey atoms represents the silver ones.

Equilibration

The pre-designed nanowire is thermal-equilibrated up to 50000 steps by incorporating the EAM potential for the concerned temperatures so that the participating atoms mimic a real system to simulate with higher accuracy.

While the "Temperature–Time Step" plot is programmed till 50000 steps, it indicates that the temperature has been equilibrated in each case by 5000 time-steps (Graph 1.). In every case, the degree of fluctuation is very high at first, escalating from 0 to some peak values, but soon, the "Temperature–Time Step" plot is damped and oscillated to

attain equilibration around the respective temperatures by 5000 time–steps and continues till 50000 steps. It is observed that the extent of fluctuation around equilibrium temperature increases with the increase in temperature.
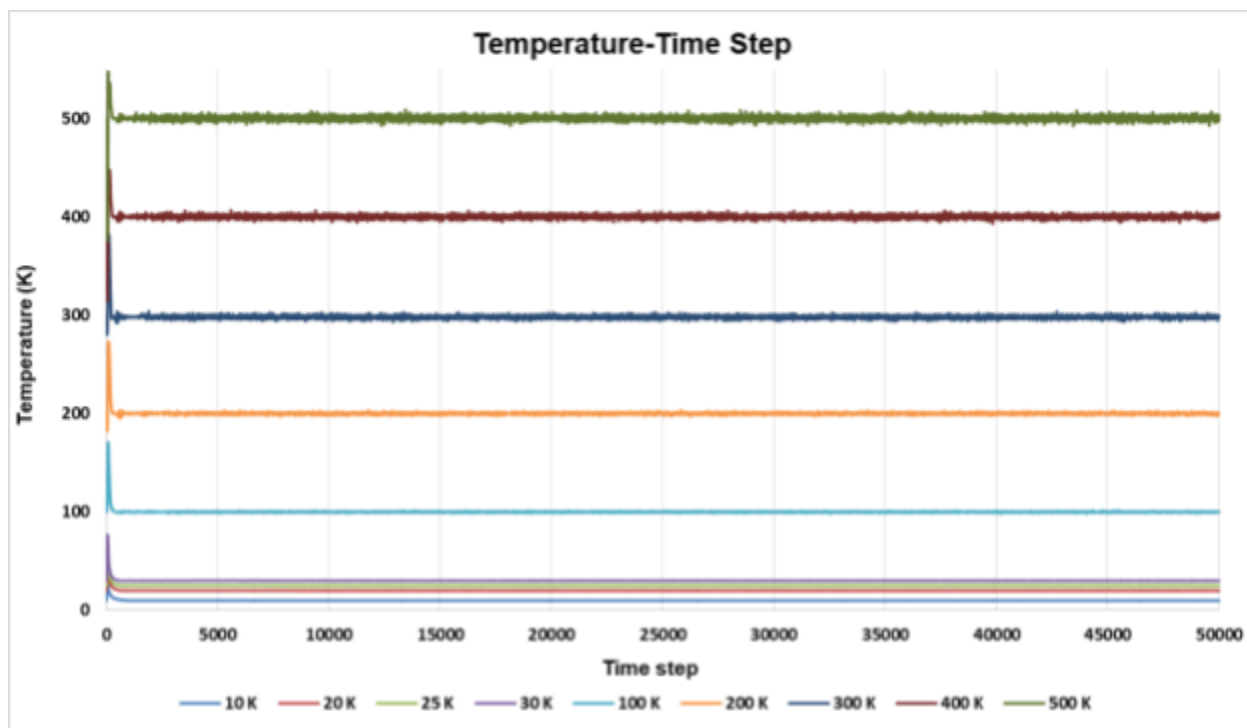
Graph 1. Temperature–Time Step of Tensile Test simulated from Molecular Dynamics in temperatures of 10 K, 20 K, 25 K, 30 K, 100 K, 200 K, 300 K, 400 K and 500 K.
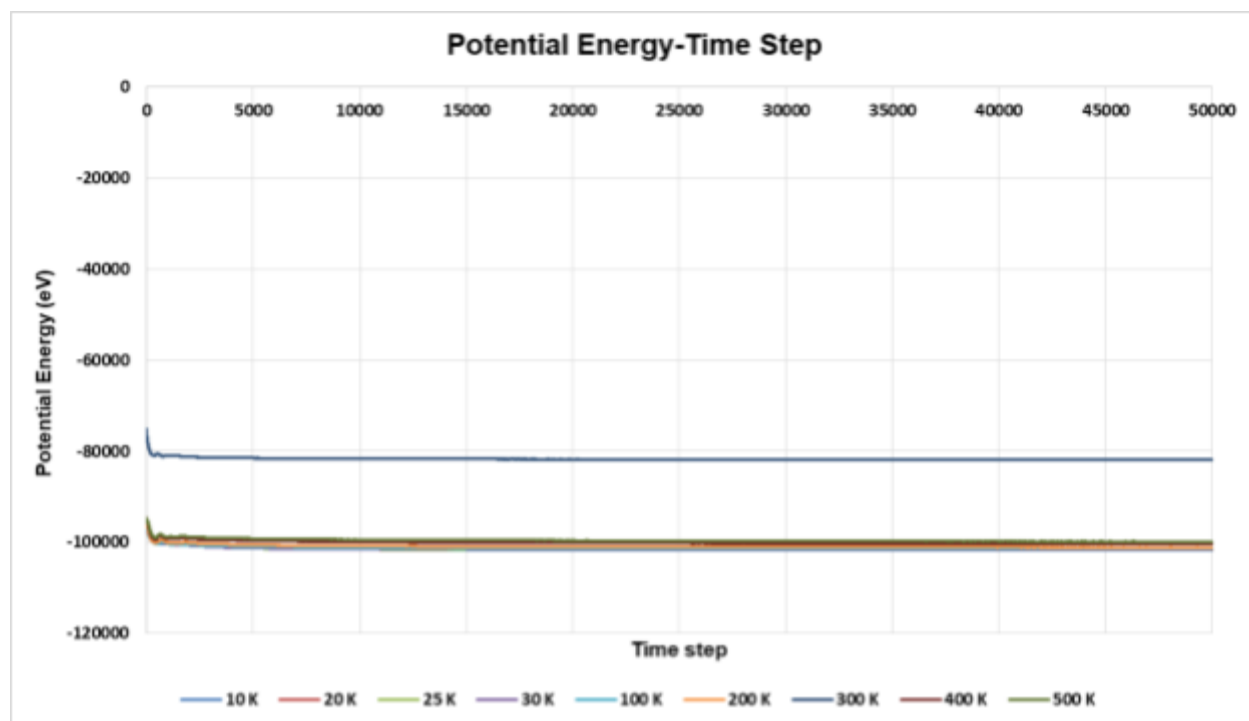
While the "Kinetic Energy-Time Step" plot is programmed till 50000 steps, it indicates that the kinetic energies associated with the structure in different temperatures are equilibrated by 20000 steps and continue till 50000 steps (Graph 2.). The degree of fluctuation is very high at first, escalating from 0 to peak values, but soon, the "Kinetic Energy-Time Step" plot is damped and oscillated to attain equilibration around the mean Kinetic Energy by 20000 time-steps in each case. It ensures that no atom in the nanostructure possesses any additional velocity, which shall otherwise hamper the test simulation. It is observed that the extent of fluctuation around equilibrium kinetic energy increases with the increasing temperature. It is also observed that the equilibrated kinetic energy increases with increasing temperature.
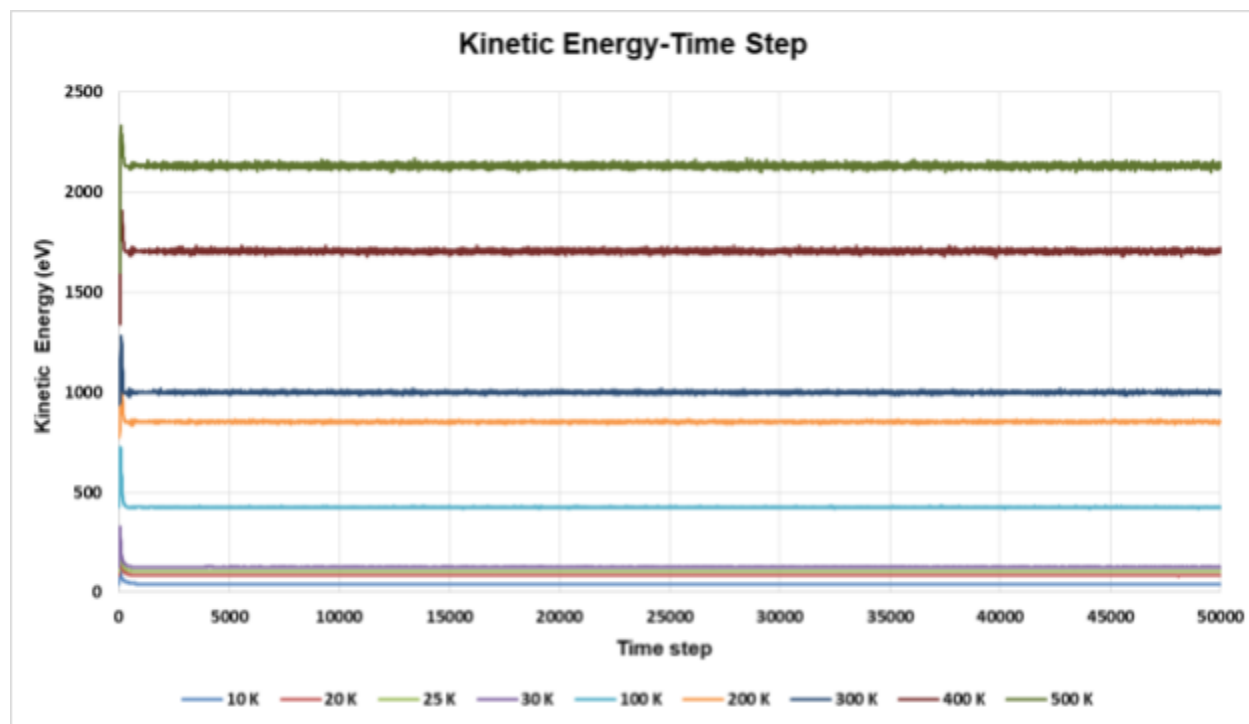
Graph 2. Kinetic Energy–Time Step of Tensile Test simulated from Molecular Dynamics in temperatures of 10 K, 20 K, 25 K, 30 K, 100 K, 200 K, 300 K, 400 K and 500 K.
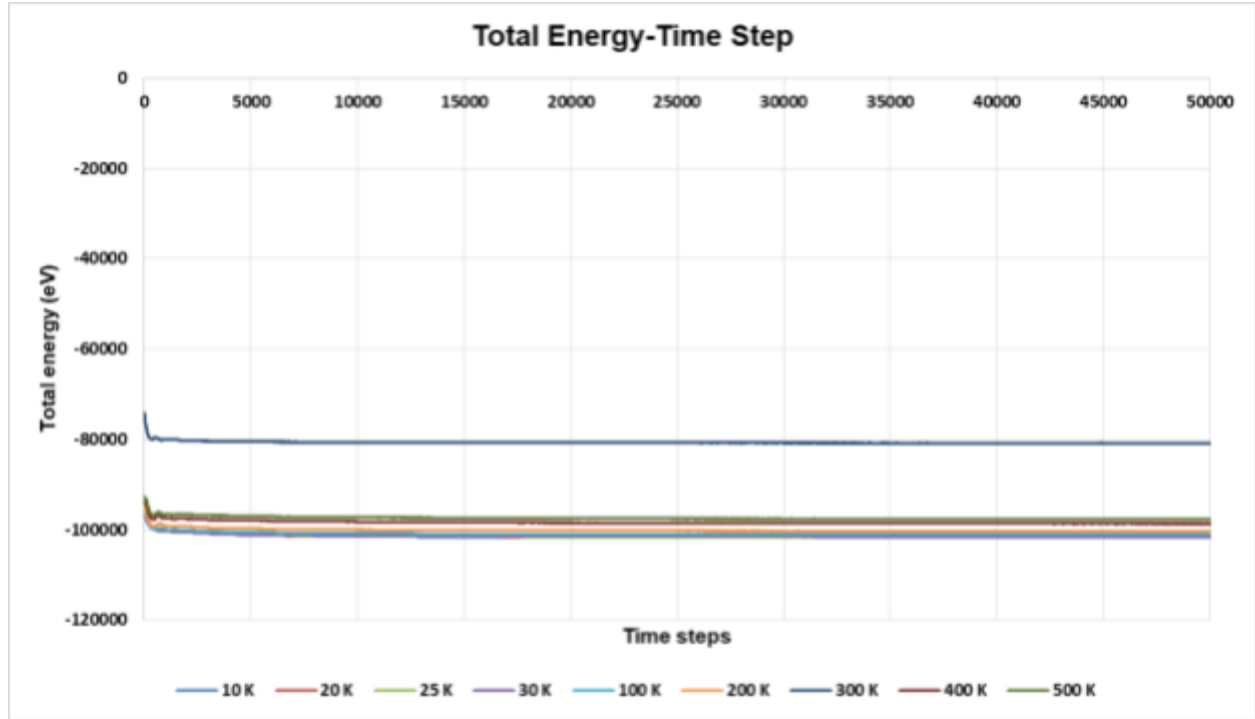
While the "Potential Energy-Time Step" plot is programmed till 50000 steps, it indicates that the potential energies associated with the structure in different temperatures are equilibrated by 20000 steps (Graph 3.). The degree of fluctuation is very high at first, falling from 0 to minimum value, but soon, the "Potential Energy-Time Step" plot is damped and oscillated to attain equilibration around equilibrated potential energy by 20000 time-steps and continues till 50000 steps. It ensures the constancy of the configuration or the shape of the nanostructure during the test simulation. In this equilibration, the stepwise fall of potential energy is observed that signifies the formation of the most stable configuration of Cu–Ag core-shell nanowire under the concerned temperatures. It is also interesting to point out that the potential energy increases with an increase in temperature from 10 K to 300 K, after which the potential energy drops till attaining 400 K and then rises till attaining 500 K.

Graph 3. Potential Energy–Time Step of Tensile Test simulated from Molecular Dynamics in temperatures of 10 K, 20 K, 25 K, 30 K, 100 K, 200 K, 300 K, 400 K and 500 K.

While the "Total Energy–Time Step" plot is programmed till 50000 steps, it indicates that the total energies associated with the structure in different temperatures are equilibrated by 20000 steps (Graph 4.). The degree of fluctuation is very high at first, falling from 0 to minimum value, but after some time, the "Total Energy–Time Step" plot is damped and oscillated to attain equilibration around equilibrated potential energies at 20000 time–steps and continues till 50000 steps. In this equilibration, the stepwise fall of total energy is observed in each case. It is also interesting to point out that the total energy increases with an increase in temperature from 10 K to 300 K, after which the total energy drops till attaining a temperature of 400 K and then rises till attaining 500 K.
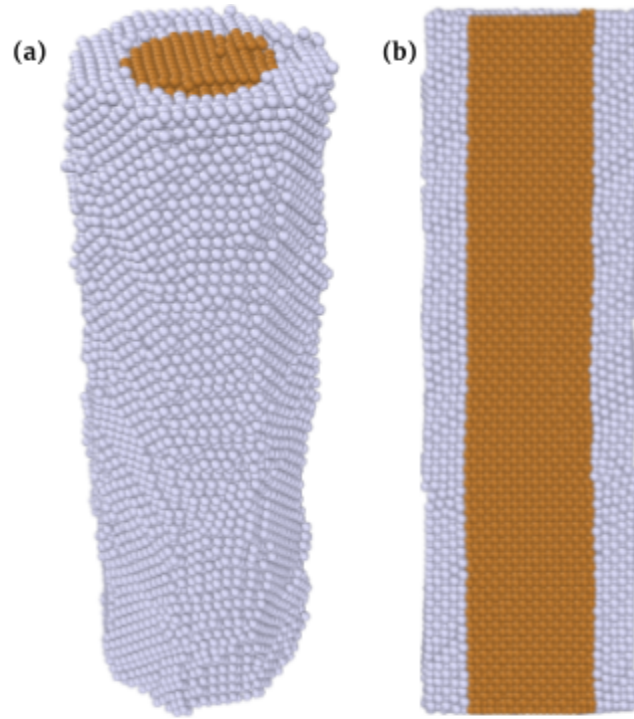
Graph 4. Total Energy–Time Step of Tensile Test simulated from Molecular Dynamics in temperature of 10 K, 20 K, 25 K, 30 K, 100 K, 200 K, 300 K, 400 K and 500 K.

The potential energy is the major contributor to the total energy in these cases, which is justified through Verlet's algorithm.

The thermal equilibrated nanowire structure is presented in Fig. 2.

Fig. 2. (a) Isometric projection and (b) sliced-section of thermally equilibrated perfect crystal of copper-silver core-shell nanowire. Here, brown atoms represent copper ones and grey atoms represents the silver ones.
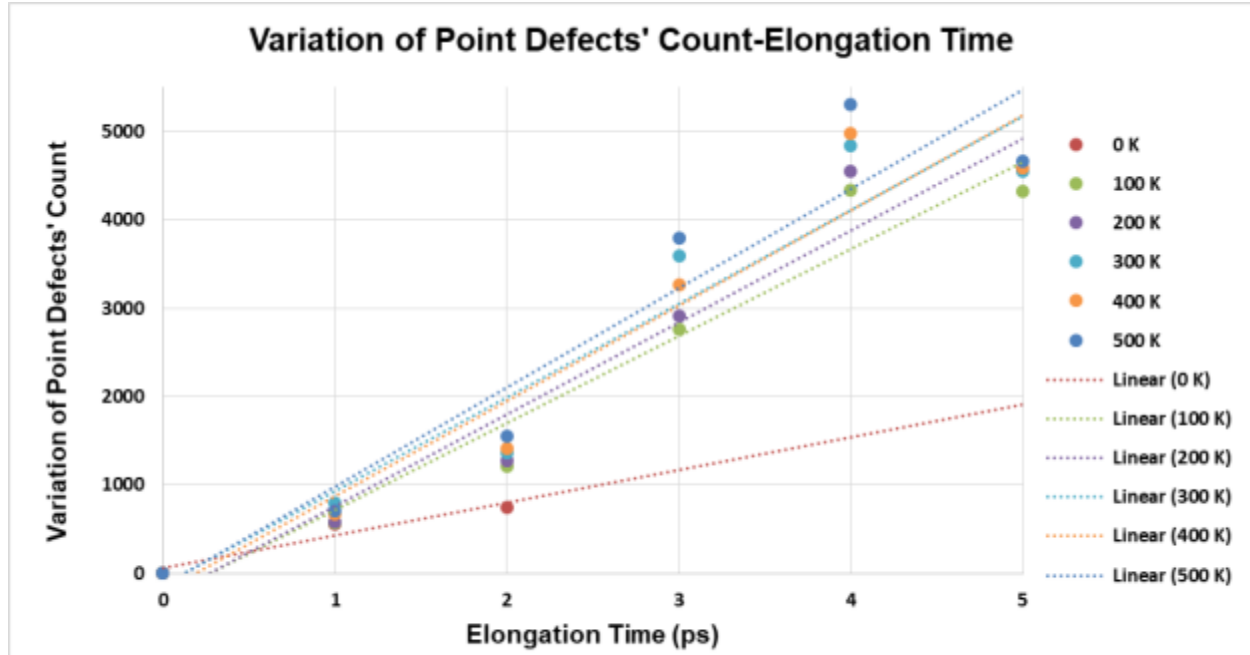
Point Defects' Count

When a material is heated, the atoms generally get excited and leave the designated lattice sites. The vacant lattice site serves as a zero-dimensional defect and is called vacancy. On the other hand, this excited atom occupies an interstitial site between the lattice points to form an interstitial. Henceforth, vacancies and interstitials constitute the point defects that are influenced by the system's temperature.

Graph 5. depicts the number of point defects after the energy equilibration in various temperatures. The point defects increase in temperature ranges of 10-100 K and 300-400 K as explained by the equation (3). However, the anomalous fall in their count in temperature ranges of 100-300 K and 400-500 K can be attributed to the vacancy-interstitial recombinations to stabilise the disparity between the tensile stress experienced by the Cu core region and the compressive stress by the Ag shell region, caused by the lattice mismatch. It is also observed from the trendline (dotted line) that the point defects, in general, increase with the increase in temperature, indicating the dominating effect of thermal excitations of the participating atoms.
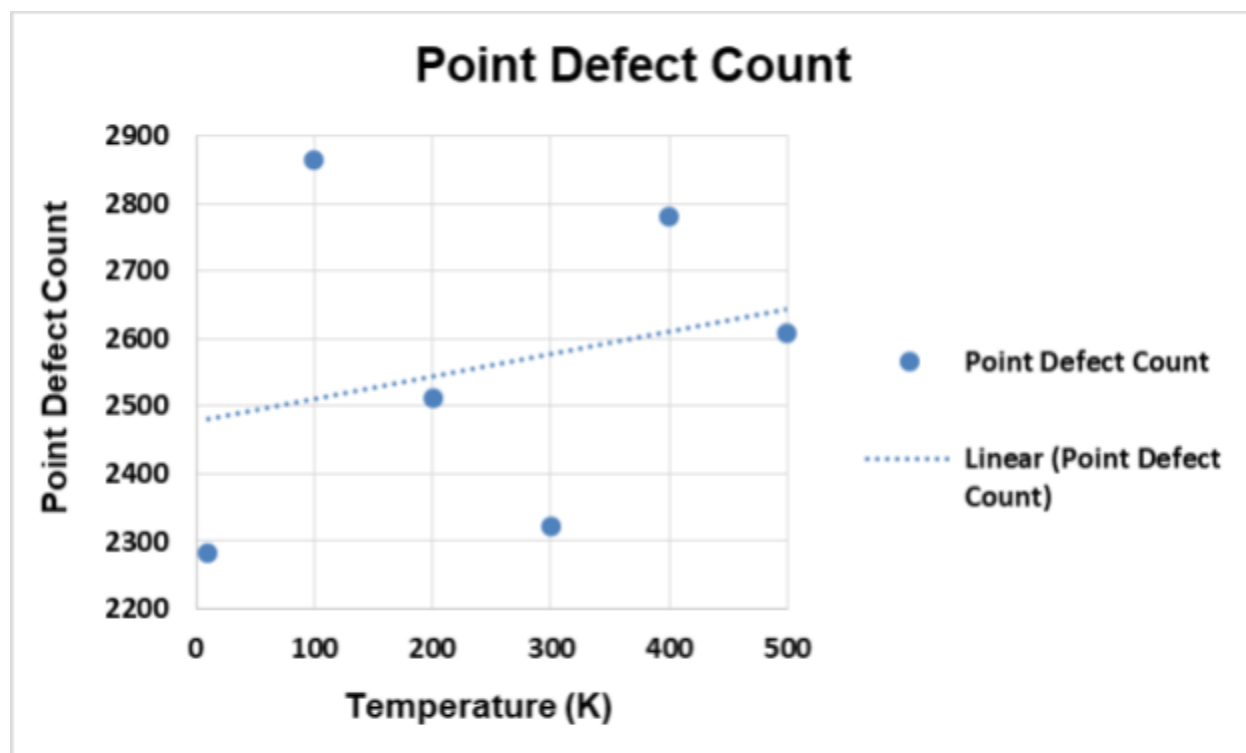
Graph 5. Point Defect Count–Temperature of the nanowire at equilibrium in temperatures of 10 K, 100 K, 200 K, 300 K, 400 K and 500 K using Molecular Dynamics.

Graph 6. depicts the variation of these point defects with respect to the elongation time from zero to the time when the strain corresponds to ultimate tensile strength for ductile fracture (in 100–500 K) and fracture strength for brittle fracture (in 10 K). Since the nanowire is simulated to undergo tensile deformation at a constant strain rate, this time is directly correlated with the strain. In each case, the end of the thermal equilibration was considered as the reference for measuring the change in point defects count while the deformation progressed. As the tensile deformation proceeds, their count increases, resulting in the nucleation of the point defects in the nanowires. With its progression, the count gradually rises from zero till it attains the strain point of ultimate tensile strength. It is also noteworthy to state the trendlines of Graph 6. suggest that the rate of increase of point defects with respect to elongation time, as observed from the corresponding slopes, increases with an increase in temperature.

Graph 6. Variation of Point Defects' Count–Elongation Time of Tensile Test simulated from Molecular Dynamics in temperatures of 10 K, 100 K, 200 K, 300 K, 400 K and 500 K.
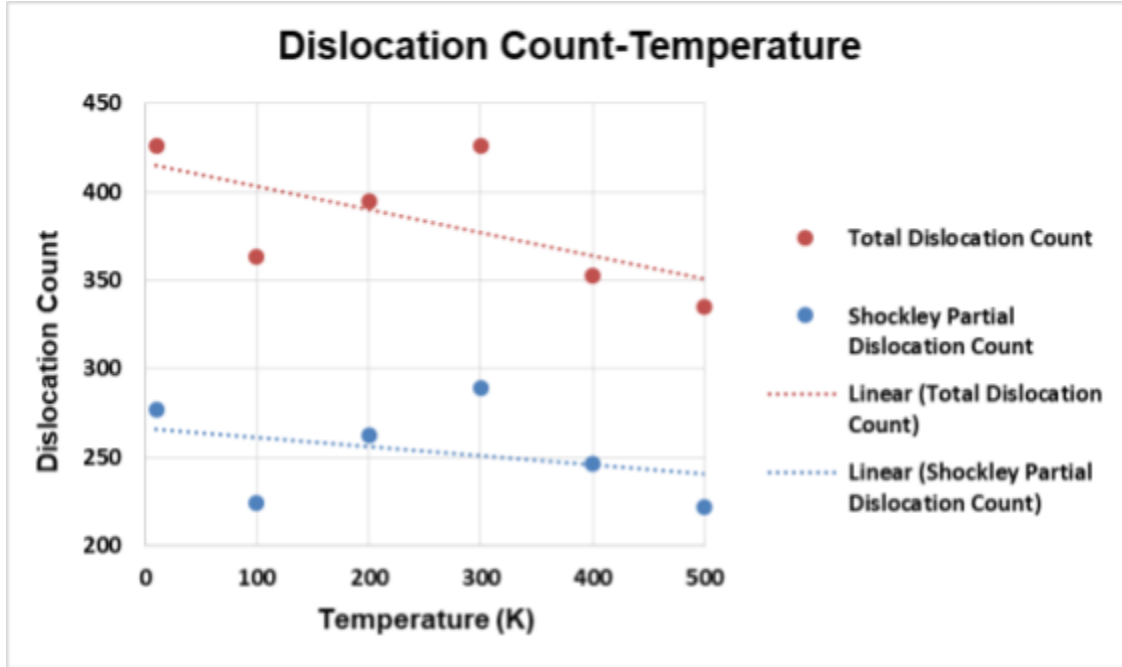
Dislocation Counts

The dislocations are the one-dimensional defects that are localised primarily in the shell region while dangling mostly from the core-shell interface of the Cu-Ag core-shell nanowire at a very low temperature. However, with the increase in temperature, the Shockley partial dislocations, developed from the interface, tend to penetrate the core. This, in turn, influences the mechanical properties gravely. This has been explained pictorially in Fig. 3.
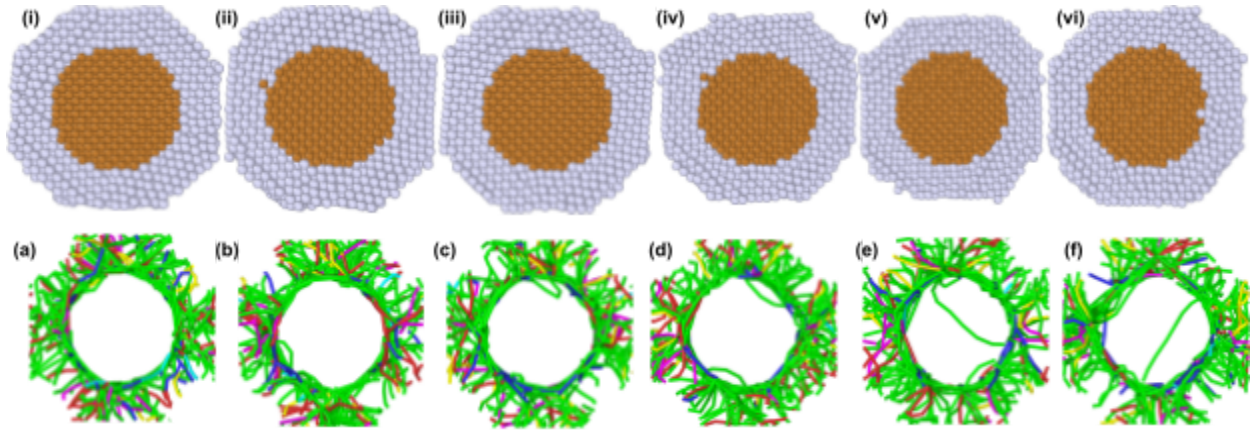
Fig. 3. Top views of (**i–vi**) Cu (brown atoms) and Ag (silver atoms) particles and (**a–f**) distribution of dislocations in core shell nanowire at 10K, 100K, 200K, 300K, 400K and 500K.

Graph 7. shows that the total dislocations' count and the Shockley partial dislocations in the nanowire first decrease from 10 K to 100 K, and then increase in temperature from 100 K to 300 K, before finally falling for the temperature from 300 K to 500 K, suggesting that the Shockley partial dislocations influence the total dislocation count. The tensile stress in the core and the compressive stress in the shell, caused by lattice mismatch, is responsible for the increase in the dislocations, particularly the Shockley partials, in the interface. As observed in Fig. 3., the core region is devoid of dislocations at a very low temperature, but the increasing temperature drives the creation of these dislocations with the increased tendency to penetrate the core. At 300 K, the Shockley partials have sufficiently penetrated the core, and so the dominating thermal excitations of the participating atoms decrease the dislocation counts from 300 K to 500 K. The decreasing trend lines of total dislocations and Shockley partials (dotted lines) in Graph 7. shows that the dominating effect of thermal excitations of the particles decreases the dislocation count with the increase in temperature. It is also observed in Fig. 4. that no dislocation exists in the region of necking in all the cases of ductile fracture.

Graph 7. Dislocation Count–Temperature (Total and Shockley partials) of the nanowire at equilibrium in temperatures of 10 K, 100 K, 200 K, 300 K, 400 K and 500 K from Molecular Dynamics.
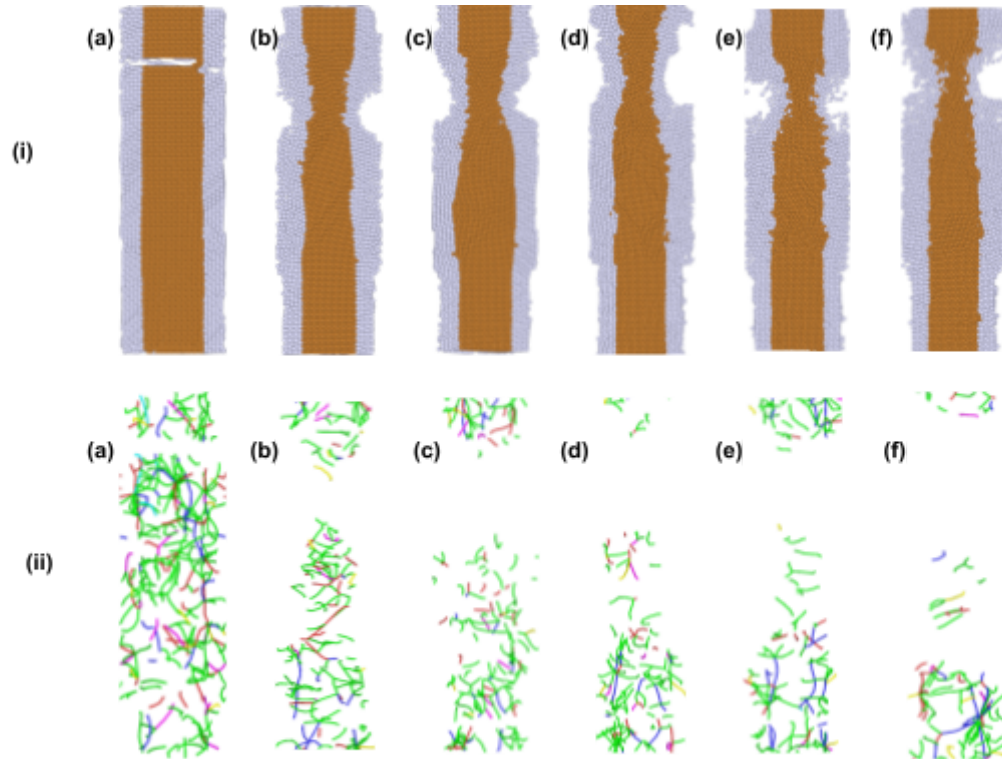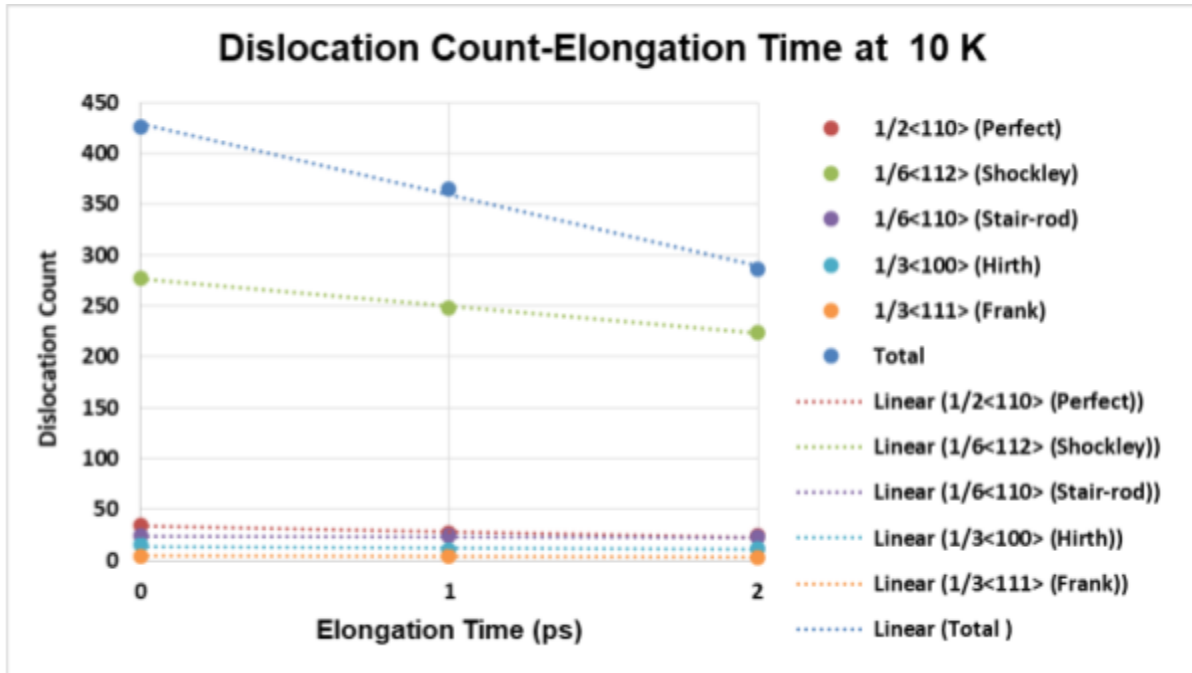

Fig. 4. **(i)** Sliced–section and **(ii)** distribution of dislocations during **(a)** brittle fracture at 10 K, and necking (in ductile fracture) at **(b)** 100 K, **(c)** 200 K, **(d)** 300K, **(e)** 400 K and **(f)** 500 K. Here, brown atoms represent copper ones and grey atoms represents the silver ones in **(i)**, while different lines in **(ii)** indicate dislocations
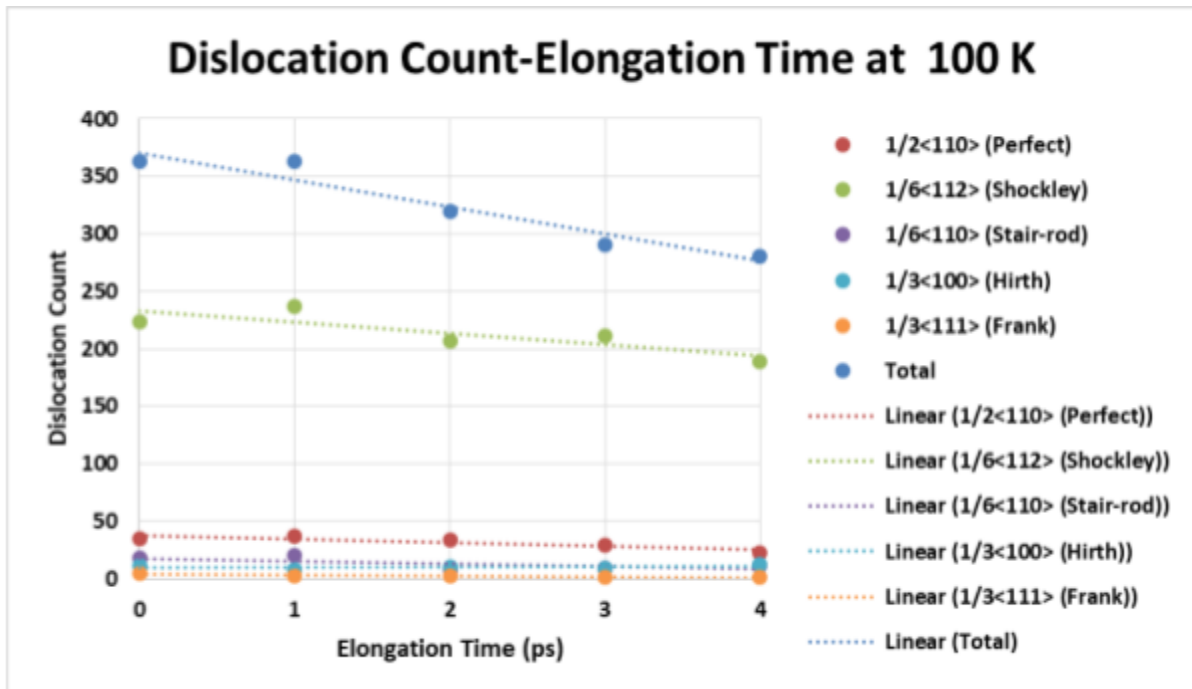
In Graph 8. (a–f), it has been observed that the Shockley partials and the perfect dislocations are major contributors to the tensile deformation process. It is observed that their counts decrease with an increase in elongation time from zero to the time when the strain corresponds to ultimate tensile strength for ductile fracture (in 100–500 K) and fracture strength for brittle fracture (in 10 K).
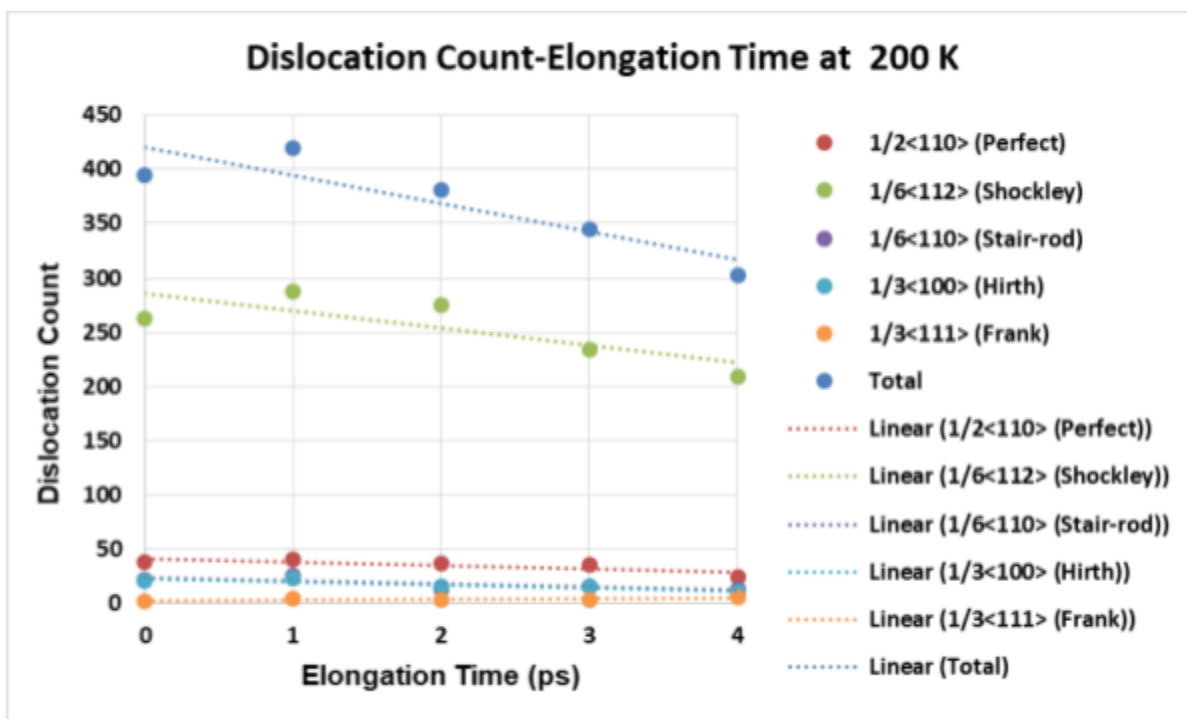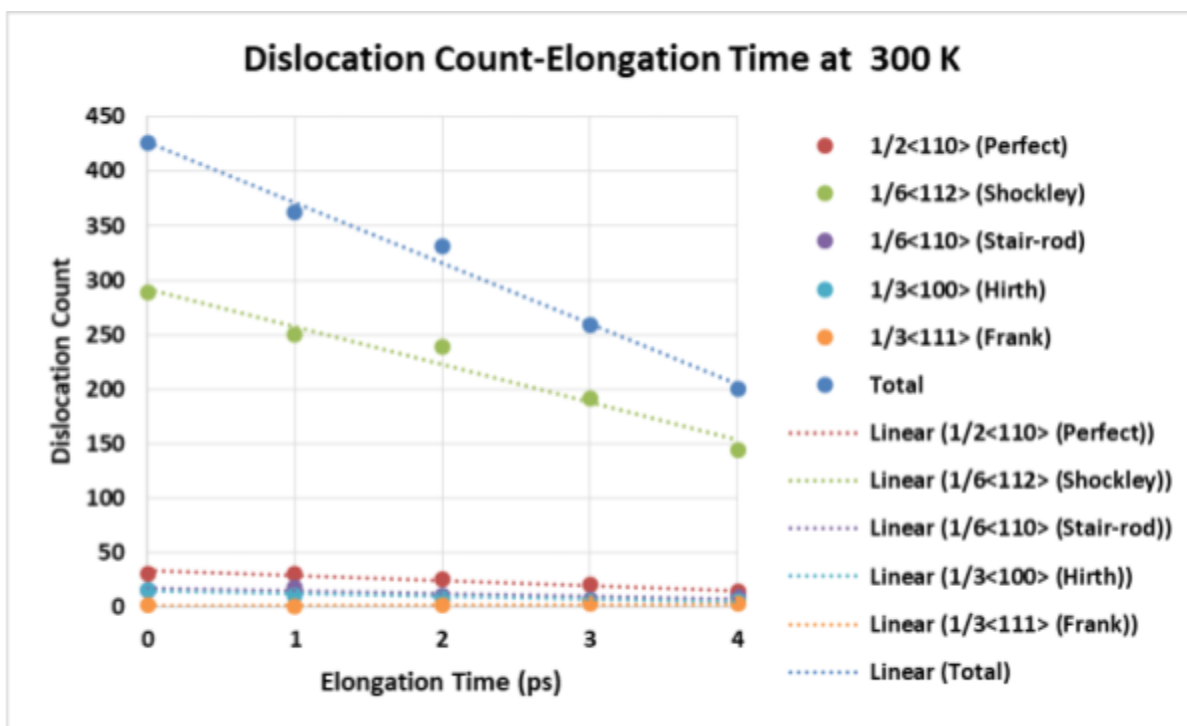

(a)

(b)

(c) Dislocation Count-Elongation Time at 200 K

(d) Dislocation Count-Elongation Time at 300 K

(e)

Dislocation Count-Elongation Time at 400 K

(f)

Dislocation Count-Elongation Time at 500 K

Graph 8. Dislocation Count–Elongation Time of the nanowire at equilibrium in temperatures of **(a)** 10 K, **(b)** 100 K, **(c)** 200 K, **(d)** 300 K, **(e)** 400 K and **(f)** 500 K using Molecular Dynamics.

In Graph 9., the total dislocation count decreases with an increase in elongation time in all the temperatures as indicated by the trendlines. This is already explained by the

influence of the Shockley partials and the perfect dislocations, which decrease with the increase in strain.

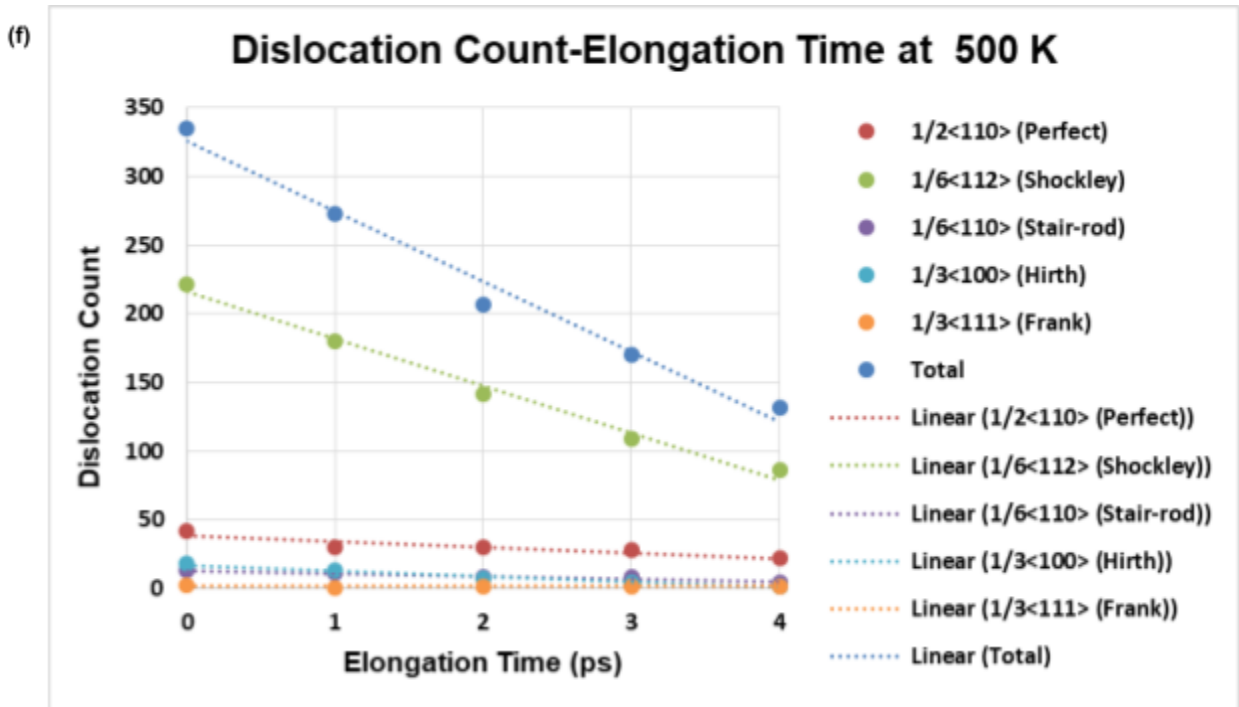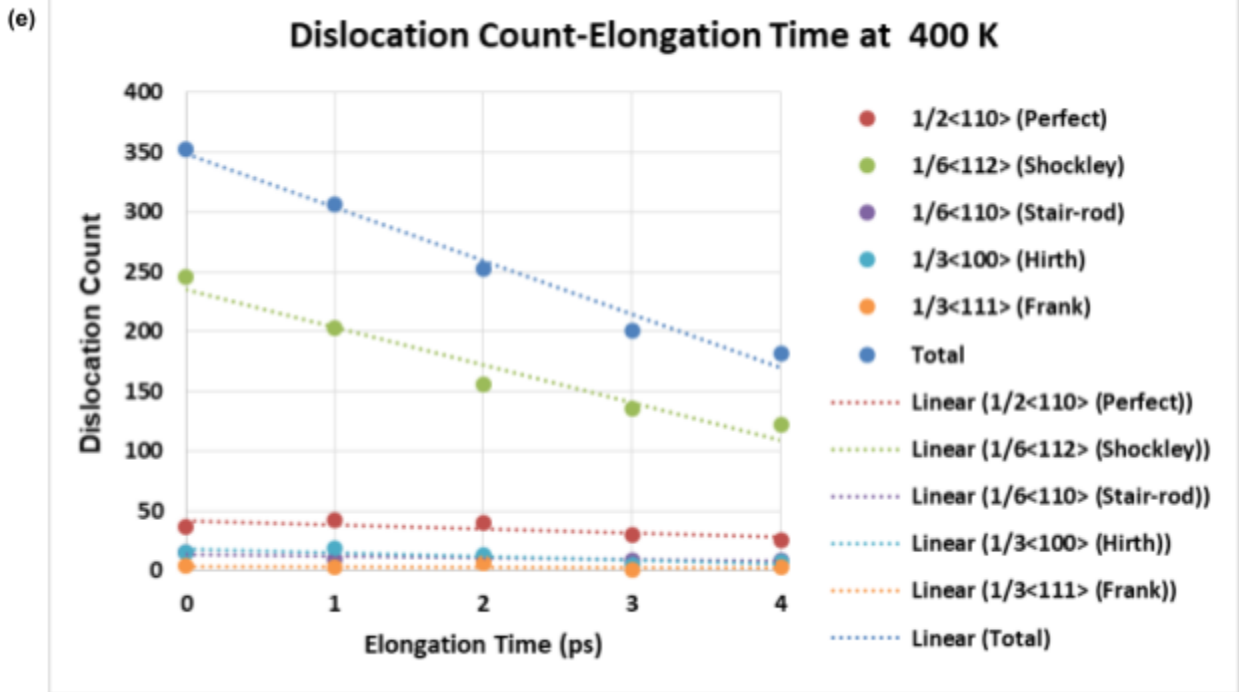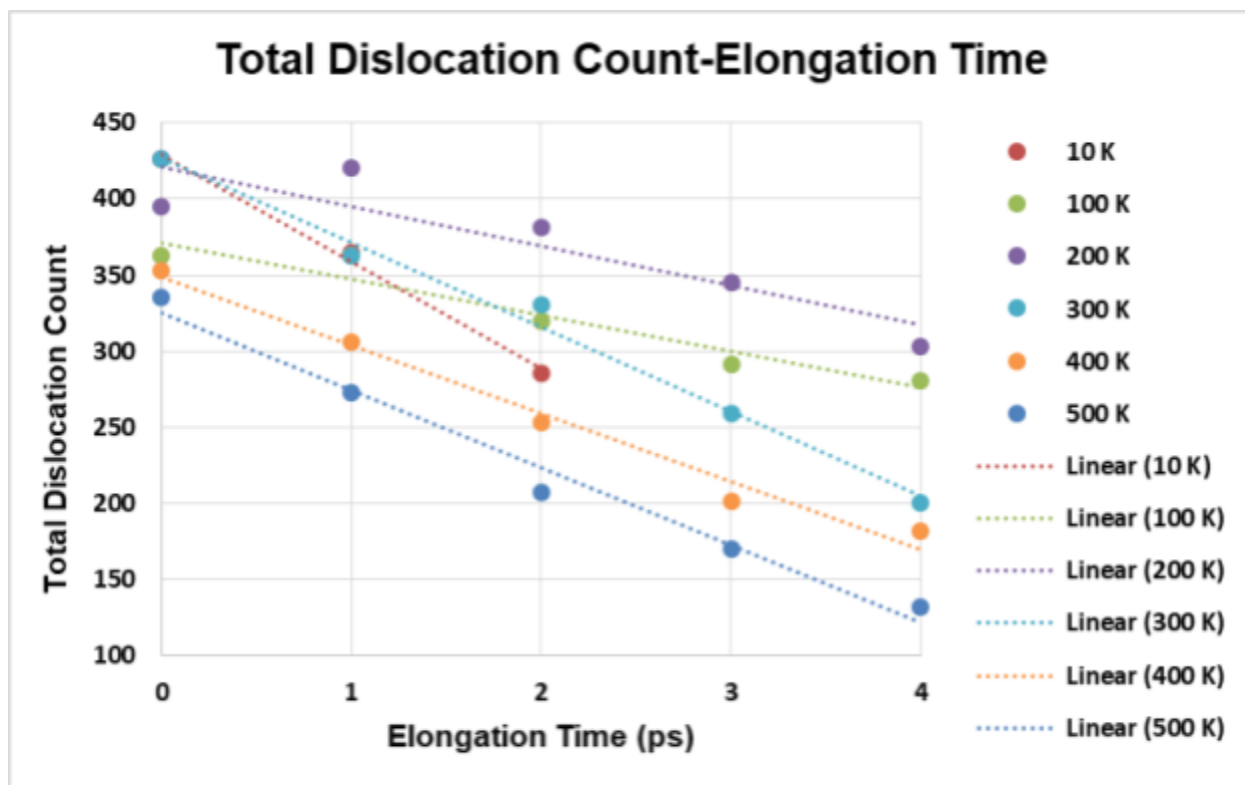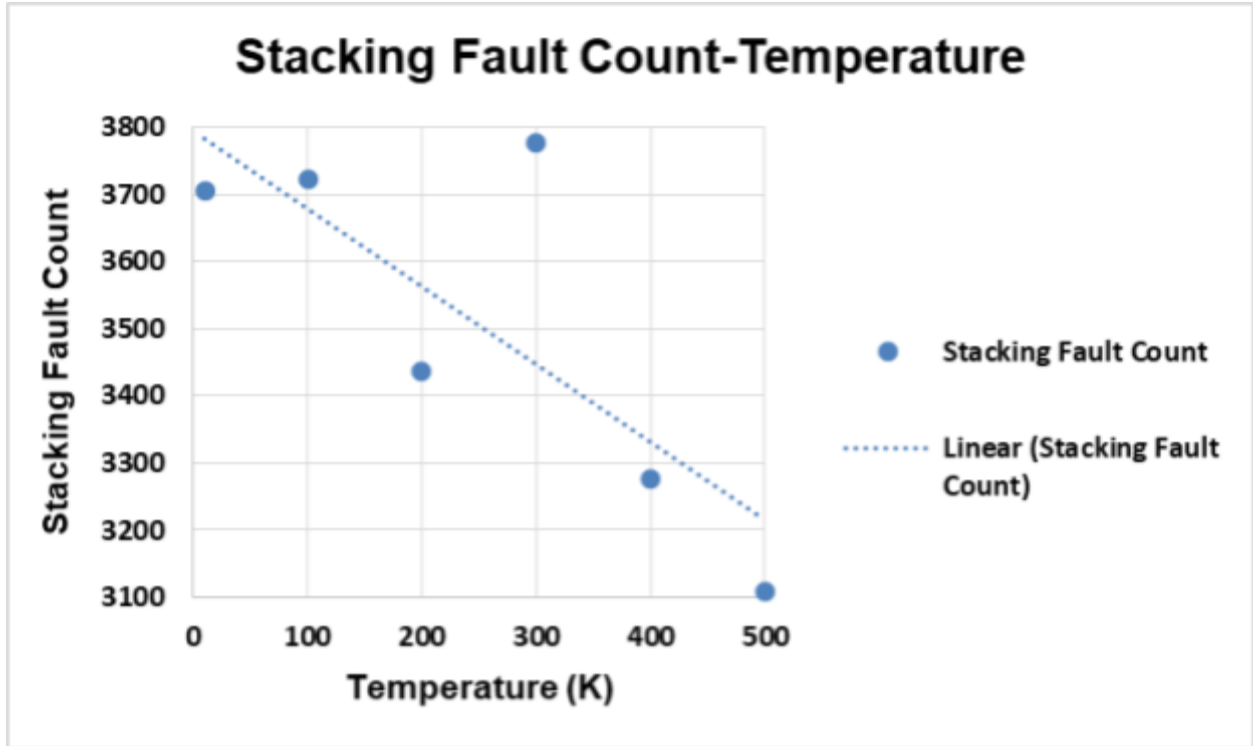**Graph 9.** Total Dislocation Count–Elongation Time of the nanowire at equilibrium in temperatures of 10 K, 100 K, 200 K, 300 K, 400 K and 500 K from Molecular Dynamics.

Stacking Fault Counts

The stacking faults are the two–dimensional defects that can be identified by the HCP arrangements in the FCC crystal. These defects occur during crystal growth, plastic deformation through the splitting of a perfect dislocation into partial dislocations, or by agglomeration of vacancies. Graph 10. depicts the variation of the number of stacking faults with respect to temperature, which can be attributed to the agglomeration of vacancies and by the energetically favourable dissociation of a perfect dislocation into the Shockley partial dislocations, governed by the Frank energy criterion to the formation of the stacking fault. However, the overall trendline suggests that the stacking fault count decreases with an increase in temperature.

Graph 10. Stacking Fault Count–Temperature of the nanowire at equilibrium in temperatures of 10 K, 100 K, 200 K, 300 K, 400 K and 500 K from Molecular Dynamics.

Fig. 5. (i)(a–d) and Fig. 5. (ii)(a–d) show that the stacking faults are mostly localised in the shell region at low temperatures (10 K, 100–300 K). However, they start to grow into the core region, as observed in 400 K and 500 K (Fig. 5. (i)(e–f) and Fig. 5. (ii)(e–f)), which is attributed to the increased penetration of Shockley partials in the core region. While it is observed that the lattice mismatch in all regions causes the loss of crystallinity in the shell region, it is equally important to highlight that high thermal excitations of atoms in 400 K and 500 K cause the core atoms to lose their crystallinity. Fig. 5. (i)(e) and Fig. 5. (ii)(e) also state that the two competitive processes, namely thermal excitations of the participating atoms and the lattice mismatch between them, show an unexpected increase in the crystallinity at 400 K.
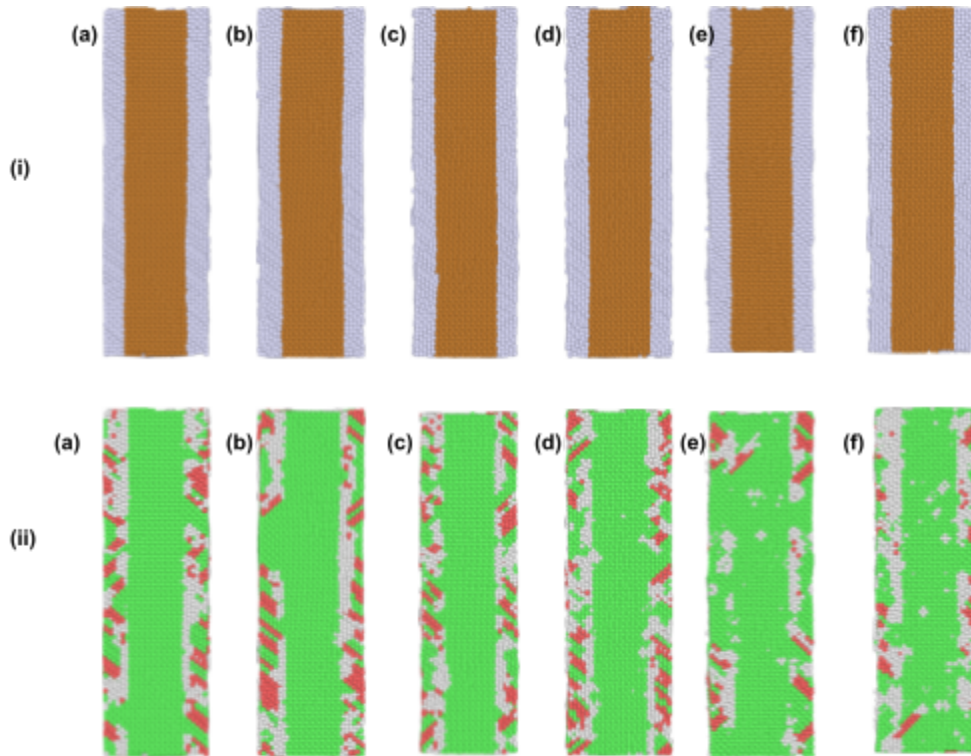
Fig. 5. (i) Sliced–section and (ii) distribution of stacking faults in unstrained nanowire (a) 10 K, (b) 100 K, (c) 200 K, (d) 300K, (e) 400 K and (f) 500 K. Here, brown atoms represent copper ones and grey atoms represents the silver ones in (i), while green atoms represent FCC, red atoms represent HCP and white atoms represent disordered in (ii).

Graph 11. depicts the variation of the number of stacking faults with respect to elongation time from zero to the time when the strain corresponds to ultimate tensile strength for ductile fracture (in 100-500 K) and fracture strength for brittle fracture (in 10 K). It is observed that the number of stacking faults reduces with an increase in strain for each temperature. It is also important to state that Fig. 6. shows that the stacking faults are observed to form near the necking regions during ductile tensile deformation (in 100-500 K).
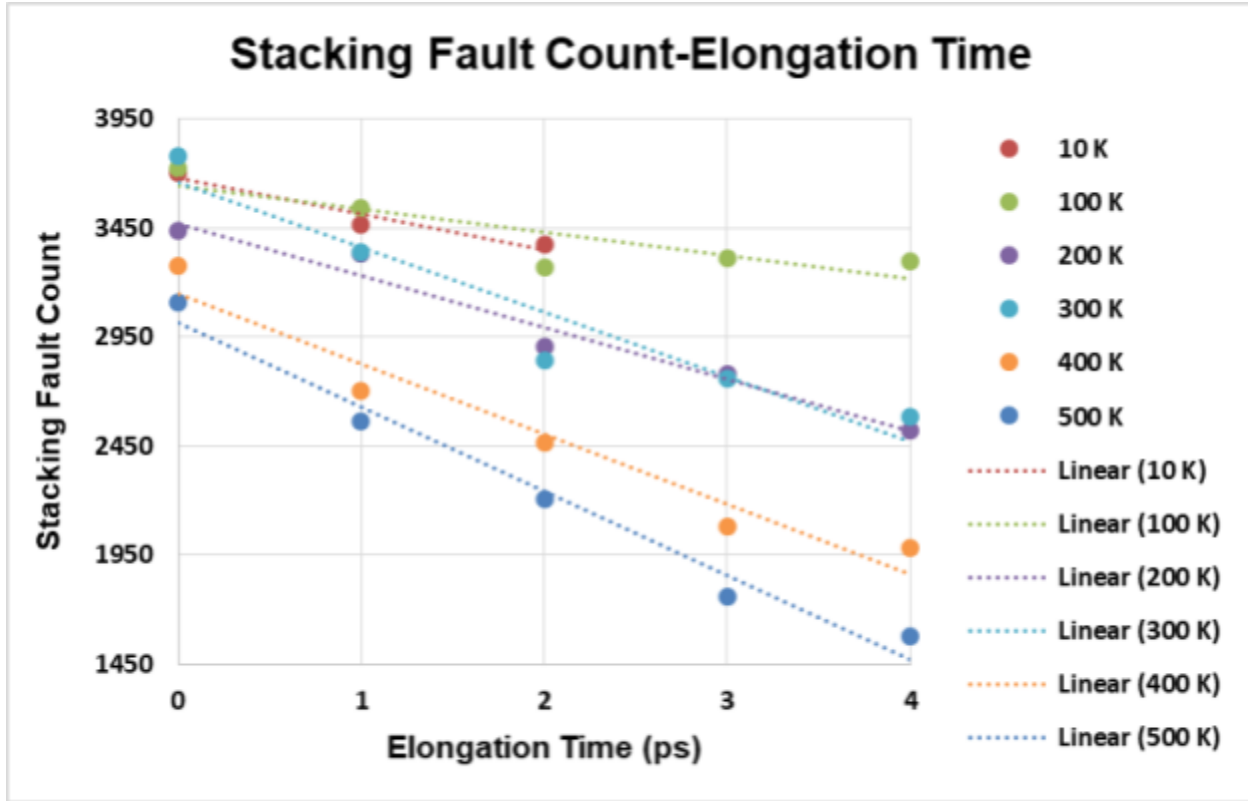
Graph 11. Stacking Fault Count–Elongation Time of Tensile Test simulated from Molecular Dynamics in temperatures of 10 K, 100 K, 200 K, 300 K, 400 K and 500 K.
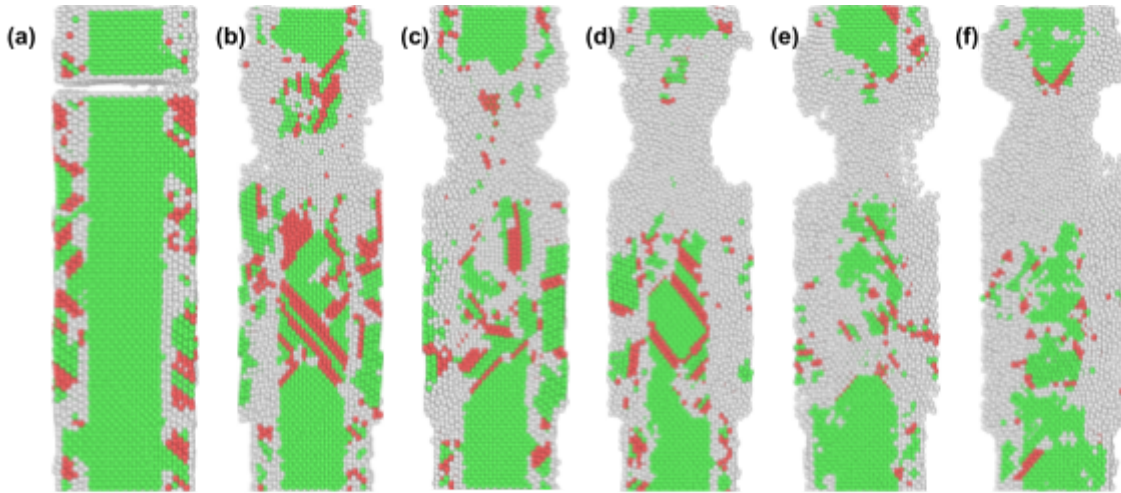
Fig. 6. Distribution of stacking faults during **(a)** brittle fracture at 10 K, and necking (in ductile fracture) at **(b)** 100 K, **(c)** 200 K, **(d)** 300K, **(e)** 400 K and **(f)** 500 K. Here, green atoms represent FCC, red atoms represent HCP and white atoms represent disordered.

Mechanical Properties

The number of vacancies, dislocations and stacking faults collectively influence the mechanical properties of the Cu–Ag core-shell nanowire. In this study, the modulus of elasticity or Young's modulus, the yield strength and the ultimate tensile strength were estimated for varying temperatures.

Graph 12. shows the stress-strain plots of the nanowire under tensile loading in temperatures of 10 K, 100 K, 200 K, 300 K, 400 K and 500 K. It was observed that the nanowire undergoes brittle failure at 10 K, while ductile failure in 100–500 K. It is also observed that the extent of elongation before fracture is highest in 300 K for its given dimensions and its compositions.
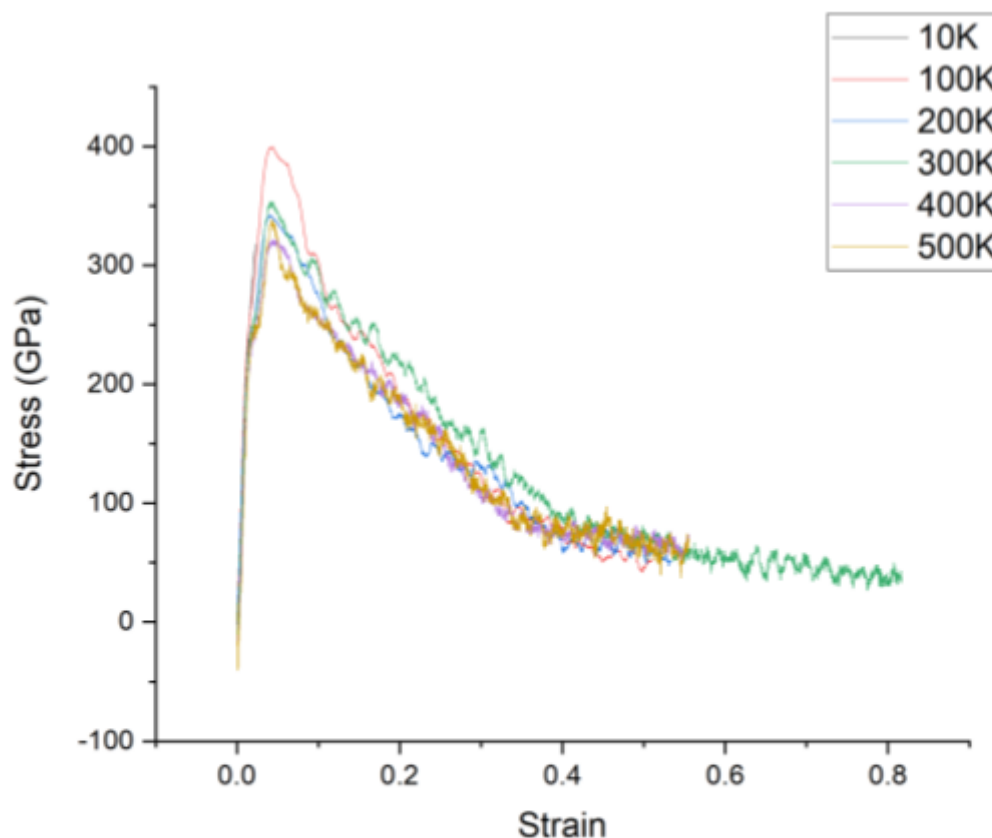
Graph 12. Stress-strain plot of the nanowire at equilibrium in temperatures of 10 K, 100 K, 200 K, 300 K, 400 K and 500 K from Molecular Dynamics.

Graph 13. (a) shows that Young's modulus decreases with an increase in temperature from 10 K to 400 K, due to the dominating effect of thermal excitations of the participating atoms. However, there is an anomalous spike in the modulus at 500 K,

due to the increased effect of the dislocations, which penetrate the core that obstructs the plastic flow.

Graph 13. (b) reports the case of yield strength anomaly, which shows that the yield strength increases rapidly from temperature 10 K to 100 K, and jaggedly from 100 K to 500 K, instead of a conventional decrease of the concerned parameter. It is to be stated that the yield strength at 10 K is exceptionally low because of the brittle fracture and so did not attain the highest possible elastic limit before experiencing the ductile failure. The jagged increase in the yield strength, i.e. the yield strength undergoes alternate increment and decrement while effectively increasing, with an increase in temperature from 100 K to 500 K. This anomaly is attributed to the increased effect of the dislocations, which penetrate the core that obstructs the plastic flow, analogous to the thermally-assisted cross-slip mechanism.

Graph 13. (c) shows the jagged decrease of ultimate tensile strength, i.e. the ultimate tensile strength undergoes alternate decrement and increment while effectively decreasing, with an increase in temperature from 100 K to 500 K, due to the competitive effects of thermal excitations of the participating atoms and the increased tendency of dislocations' penetration into the core from the interface. However, the effective decrease of the parameter is attributed to the dominance of the earlier effect over the latter.
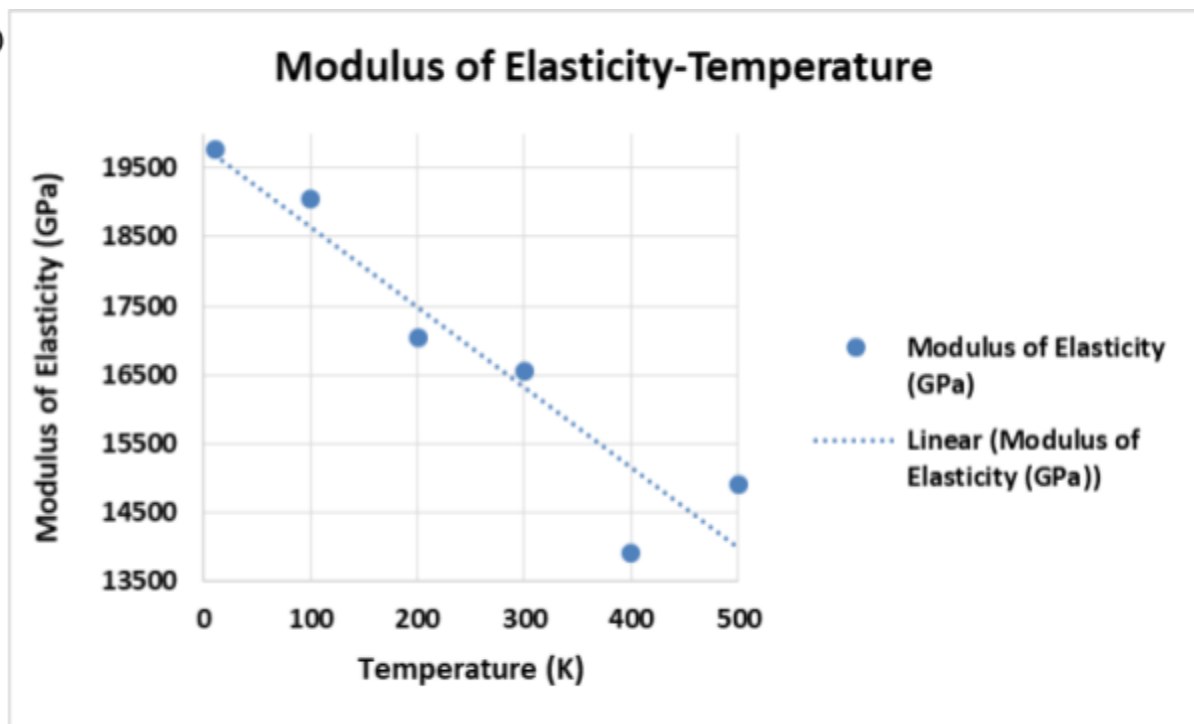
(b)
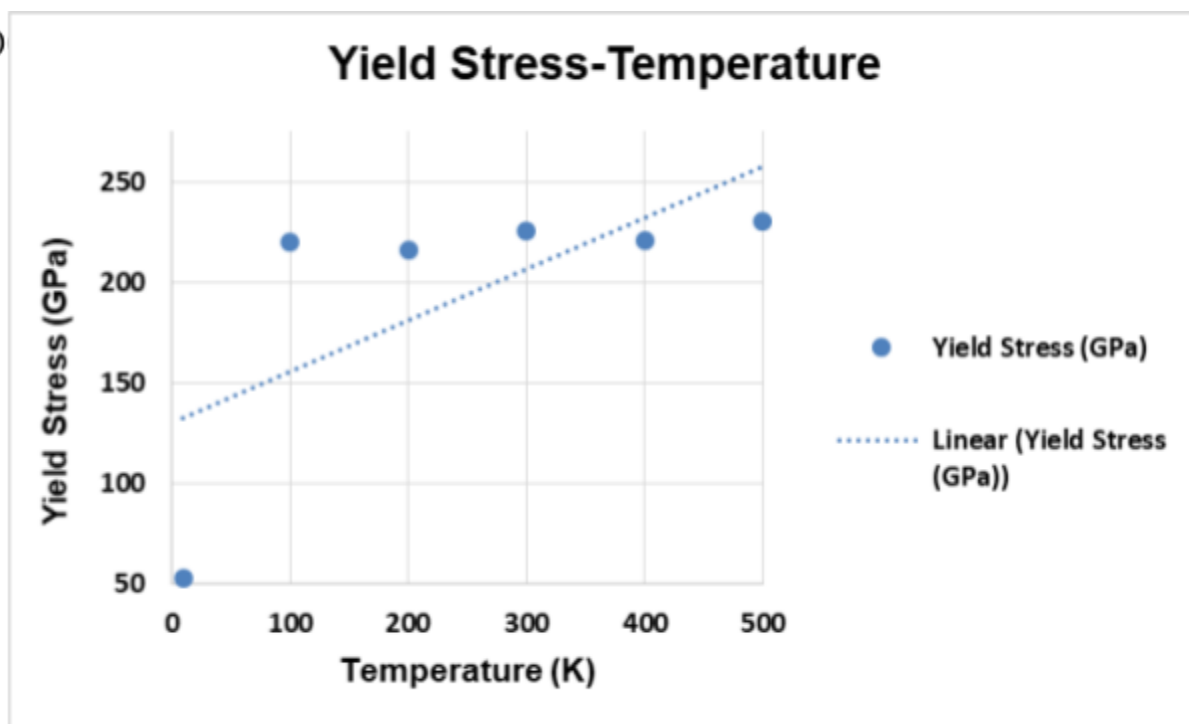
(c)
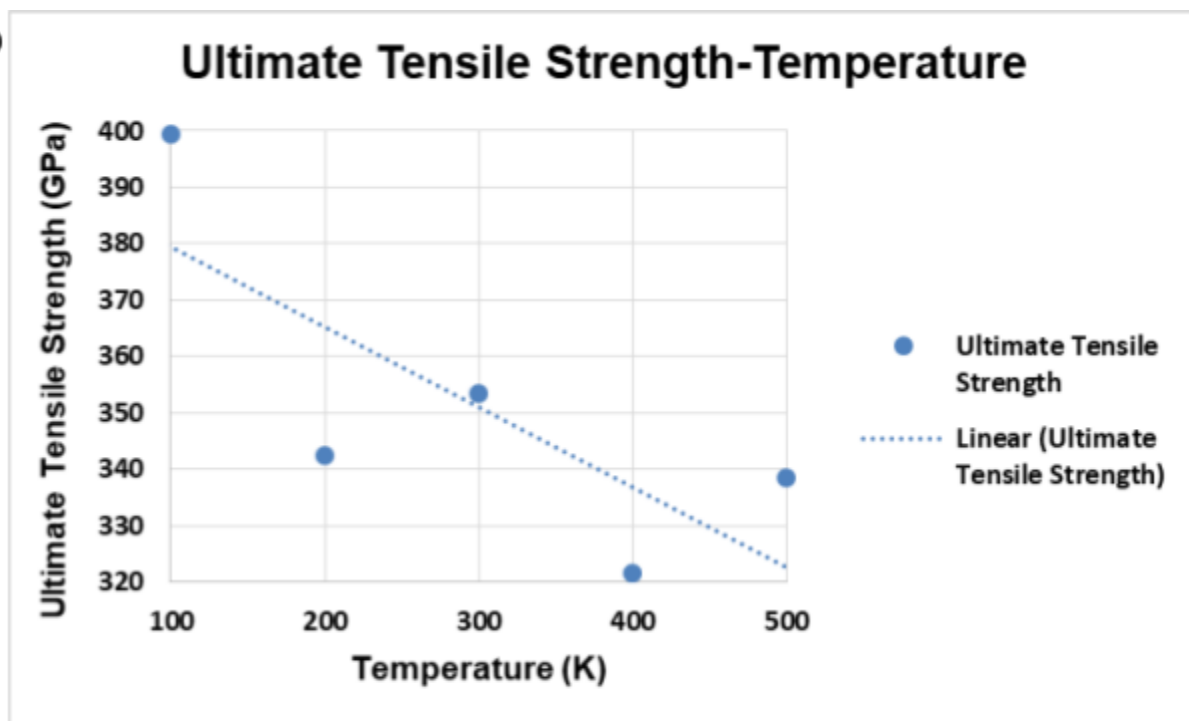
Graph 13. (a) Modulus of Elasticity–Temperature, **(b)** Yield Stress–Temperature and **(c)** Ultimate Tensile Strength–Temperature of the nanowire at equilibrium in temperatures of 10 K, 100 K, 200 K, 300 K, 400 K and 500 K using Molecular Dynamics.

Ductile to Brittle Transition Temperature

While the core-shell nanowire experiences the brittle fracture in 10 K, it experiences ductile fracture in 100-500K. Thus, the tensile deformation of the concerned nanowire is simulated with the aforementioned dimensions at temperatures of 10 K, 20 K, 25 K and 30 K. In Fig. 7. (a-d), it was observed that the nanowire undergoes brittle failure in 10 K, 20 K and 25 K, and ductile failure in 30 K. This indicates that the ductile-to-brittle transition temperature of the copper-silver core-shell nanowire of 40 Å core diameter and 10 Å shell thickness for a strain rate of 2 Å/ps is 25-30 K.
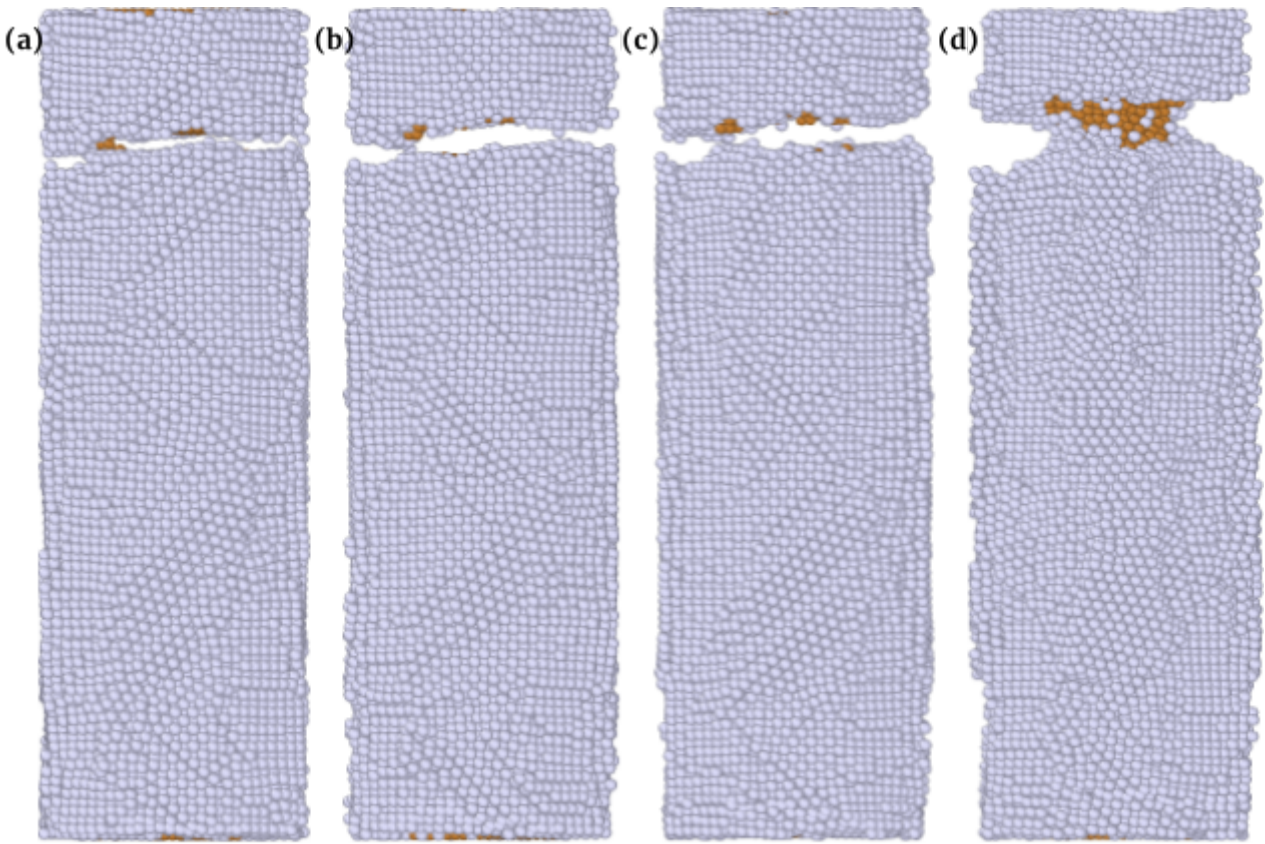
Fig. 7. Nanowire experience brittle fractures in **(a)** 10 K, **(b)** 20 K and **(c)** 25 K, while ductile fracture (and so necking is observed) in **(d)** 30 K.

Conclusion

Conclusion

In this study, the following conclusions are established:

- An increase in the temperature surges the degree of thermal fluctuations around its equilibrated temperature, due to the thermal excitations of the participating atoms that serve as the measure of the temperature of the system. This also increases the extent of fluctuations in the mean kinetic energy of the atoms. It is also worth noting that the temperature directly influences kinetic energy.

- An increase in the temperature increases the mean potential energy and the mean total energy of the atoms towards the end of thermal equilibration, which indicates the increase in the instability of the nanowire. However, it was observed that the nanowire shows exceptional instability with the sudden increase in the potential energy at 300 K.

- While the point defects experience an increase in 10-100 K and 300-400 K due to the dominance of the thermal excitations of the participating atoms, they decrease in the temperature range of 100-300 K and 400-500 K due to the dominance of lattice mismatch between the atoms of the core and shell in the interface. The point defects are also observed to increase with the increase in the strain of the nanowire during the tensile testing simulation at each temperature.

- The dislocations are observed to be localised in the shell region and dangle from the core-shell interface of the nanowire at low-temperature. But as the temperature increases, the dislocations, particularly Shockley partial, bound from the core-shell interface tend to penetrate the core region, which is visible in 300K. Further, a decrease in the number of Shockley partials and perfect dislocations during tensile strain at different temperatures are observed.

- The number of stacking faults in the copper-silver core-shell nanowire of core diameter of 40 Å, shell thickness of 10 Å and length of 200 Å, are influenced by the agglomeration of vacancies and the dissociation of perfect dislocation into the Shockley partials Further, a decrease in the number of stacking faults during tensile strain at different temperatures is observed. It has also been observed that the stacking faults are mostly localised in the shell region at low temperatures (10 K, 100-300 K) due to the lattice mismatch, while they

penetrate the core region at higher temperatures (400-500 K) due to penetration of stacking fault into the core. This nanowire at 400 K shows an unexpected increase in the crystallinity due to thermal excitations of the participating atoms and the lattice mismatch between them. During straining at 2 Å/ps, the stacking faults are observed to form near the neck region during ductile fracture in 100-500 K.

- The stress-strain plot indicates that the Cu-Ag core-shell nanowire with a core diameter of 40 Å and a shell thickness of 10 Å for a strain rate of 2 Å/ps experiences the longest elongation before fracture at 300 K.

- The Young's Modulus decreases with an increase in temperature from 100 K to 400K, and then it increases slightly at 500 K. While the fall in Young's Modulus can be attributed to the increased effect of thermal excitations, the anomalous increment at 500K is designated to the significant increase in the penetration of Shockley partials and perfect dislocations from the core-shell interface into the core-region that enhances the strengthening effect in the nanowire.

- The abnormal low yield point of the nanowire at 10 K can be attributed to the brittle fracture, the following anomalous increment, known as the Yield Point Anomaly, for those is quite slow and jagged, which is attributed to the increased effect of the dislocations, which penetrated the core that obstructs the plastic flow, analogous to the thermally-assisted cross-slip mechanism.

- The ultimate tensile strength decreases jaggedly with an increase in temperature, due to the occurrence of competing processes, namely thermal excitation of the participating atoms and the increased tendency of penetration of Shockley partials and perfect dislocations from the core-shell interface to the core region in these temperatures.

- The ductile-to-brittle transition temperature is reported to take place at 25-30 K in the Cu-Ag core-shell nanowire with a core diameter of 40 Å and a shell thickness of 10 Å for a strain rate of 2 Å/ps.

This work shall, thus, serve as the guiding manual to the development of new nanomaterials whose applications shall involve the variation of temperatures, namely structural applications in aerospace, defence and nuclear sectors.

Future Scopes

This work can be extended in the following directions:

- The atomistic changes and the variations in mechanical properties involved in the copper–silver core-shell nanowires and their composites of different dimensions and temperatures under compressive, torsion and fatigue loading using molecular dynamics can be investigated.
- The atomistic changes and the variations in mechanical properties involved in the copper–silver core-shell nanowires and their composites of different dimensions and temperatures under normal, tensile, compressive, torsion and fatigue loading during corrosion using reactive molecular dynamics can be investigated.
- The changes in electronic and optical properties involved in the copper–silver core-shell nanowires and their composites of different dimensions and temperatures under normal, tensile, compressive, torsion and fatigue loading in presence of normal and corrosive environments using density functional theory can be investigated.

References

1. Hulla, J. E., Sahu, S. C., & Hayes, A. W. (2015). Nanotechnology: History and future. *Human & experimental toxicology*, *34*(12), 1318-1321.

2. Buzea, C., Pacheco, I. I., & Robbie, K. (2007). Nanomaterials and nanoparticles: sources and toxicity. *Biointerphases*, *2*(4), MR17-MR71.

3. Feynman, R. P. (1959). There's plenty of room at the bottom. *Engineering and science*, *23*(5).

4. Selin, C. (2007). Expectations and the Emergence of Nanotechnology. *Science, Technology, & Human Values*, *32*(2), 196-220.

5. Taniguchi, N. (1974). On the basic concept of nanotechnology. *Proceeding of the ICPE*.

6. Binnig, G., & Rohrer, H. (1982). *U.S. Patent No. 4,343,993*. Washington, DC: U.S. Patent and Trademark Office.

7. Binnig, G., Quate, C. F., & Gerber, C. (1986). Atomic force microscope. *Physical review letters*, *56*(9), 930.

8. Sadewasser, S., & Glatzel, T. (2012). *Kelvin probe force microscopy* (Vol. 48, pp. 201-204). Berlin: Springer.

9. Toxvaerd, S., Heilmann, O. J., & Dyre, J. C. (2012). Energy conservation in molecular dynamics simulations of classical systems. *The Journal of chemical physics*, *136*(22), 224106.

10. Fermi, E., Pasta, J., & Ulam, S. (1955). Los Alamos report No. LA–1940, *Appl. Math*, *15*, 143.

11. Gibson, J. B., Goland, A. N., Milgram, M., & Vineyard, G. (1960). Dynamics of radiation damage. *Physical Review*, *120*(4), 1229.

12. Rahman, A. (1964). Correlations in the motion of atoms in liquid argon. *Physical review*, *136*(2A), A405.

13. Khan, I., Saeed, K., & Khan, I. (2019). Nanoparticles: Properties, applications and toxicities. *Arabian journal of chemistry*, *12*(7), 908-931.

14. https://en.wikipedia.org/wiki/Nanowire

15. https://physics.nist.gov/cgi-bin/cuu/Value?rk

16. Pidgeon, N., Porritt, J., Ryan, J., Seaton, A., Tendler, S., Welland, M., & Whatmore, R. (2004). Nanoscience and nanotechnologies: opportunities and uncertainties. *The Royal Society, The Royal Academy of Engineering*, *29*(07), 2004.

17. Xia, X., Wang, Y., Ruditskiy, A., & Xia, Y. (2013). 25th Anniversary Article: Galvanic replacement: a simple and versatile route to hollow nanostructures with tunable and well‑controlled properties. *Advanced Materials*, *25*(44), 6313-6333.

18. Stewart, I. E., Ye, S., Chen, Z., Flowers, P. F., & Wiley, B. J. (2015). Synthesis of Cu–Ag, Cu–Au,

and Cu–Pt core–shell nanowires and their use in transparent conducting films. *Chemistry of Materials*, *27*(22), 7788-7794.

19. Ye, S., Rathmell, A. R., Stewart, I. E., Ha, Y. C., Wilson, A. R., Chen, Z., & Wiley, B. J. (2014). A rapid synthesis of high aspect ratio copper nanowires for high-performance transparent conducting films. *Chemical communications*, *50*(20), 2562-2564.

20. Wei, Y., Chen, S., Lin, Y., Yang, Z., & Liu, L. (2015). Cu–Ag core–shell nanowires for electronic skin with a petal molded microstructure. *Journal of Materials Chemistry C*, *3*(37), 9594-9602.

21. Stewart, I. E., Ye, S., Chen, Z., Flowers, P. F., & Wiley, B. J. (2015). Synthesis of Cu–Ag, Cu–Au, and Cu–Pt core–shell nanowires and their use in transparent conducting films. *Chemistry of Materials*, *27*(22), 7788-7794.

22. Wang, J., & Shin, S. (2017). Sintering of multiple Cu–Ag core–shell nanoparticles and properties of nanoparticle-sintered structures. *Rsc Advances*, *7*(35), 21607-21617.

23. Ma, C., Xue, S., Bridges, D., Palmer, Z., Feng, Z., & Hu, A. (2017). Low temperature brazing nickel with Ag nanoparticle and Cu-Ag core-shell nanowire nanopastes. *Journal of Alloys and Compounds*, *721*, 431-439.

24. Sarkar, J., & Das, D. K. (2018). Study of the effect of varying core diameter, shell thickness and strain velocity on the tensile properties of single crystals of Cu–Ag core–shell nanowire using molecular dynamics simulations. *Journal of Nanoparticle Research*, *20*(1), 1-10.

25. Sarkar, J., & Das, D. K. (2018). Molecular dynamics study of defect and dislocation behaviors during tensile deformation of copper-silver core-shell nanowires with varying core diameter and shell thickness. *Journal of Nanoparticle Research*, *20*(10), 1-12.

26. Cruz, M. A., Ye, S., Kim, M. J., Reyes, C., Yang, F., Flowers, P. F., & Wiley, B. J. (2018). Multigram synthesis of Cu-Ag Core–shell nanowires enables the production of a highly conductive polymer filament for 3D printing electronics. *Particle & Particle Systems Characterization*, *35*(5), 1700385.

27. Weng, W. L., Hsu, C. Y., Lee, J. S., Fan, H. H., & Liao, C. N. (2018). Twin-mediated epitaxial growth of highly lattice-mismatched Cu/Ag core–shell nanowires. *Nanoscale*, *10*(21), 9862-9866.

28. Zhang, B., Li, W., Jiu, J., Yang, Y., Jing, J., Suganuma, K., & Li, C. F. (2019). Large-scale and galvanic replacement free synthesis of Cu@ Ag core–shell nanowires for flexible electronics. *Inorganic chemistry*, *58*(5), 3374-3381.

29. Sarkar, J., & Ganguly, S. (2022). Investigation of the thermal properties of Cu–Ag core-shell nanowires using molecular dynamics simulation. *Physica B: Condensed Matter*, 413876.

30. Wang, S., Shan, Z., & Huang, H. (2017). The mechanical properties of nanowires. *Advanced Science*, *4*(4), 1600332.

31. Gaskell, D. R., & Laughlin, D. E. (2017). *Introduction to the Thermodynamics of Materials*. CRC press.

32. Dieter, G. E. (1988). Mechanical metallurgy (2001). *SI Metric Edition*.

33. Hull, D., & Bacon, D. J. (2011). *Introduction to dislocations* (Vol. 37). Elsevier.

34. Hirth, J. P., & Lothe, J. (1982). Theory of dislocations. Wiley. *New York*, 376.

35. Fine, M. E. (1973). Introduction to chemical and structural defects in crystalline solids. In *The Chemical Structure of Solids* (pp. 283-333). Springer, New York, NY.

36. Li, B., Yan, P. F., Sui, M. L., & Ma, E. (2010). Transmission electron microscopy study of stacking faults and their interaction with pyramidal dislocations in deformed Mg. *Acta Materialia*, *58*(1), 173-179.

37. https://en.wikipedia.org/wiki/Stacking_fault

38. LeSar, R. (2013). *Introduction to computational materials science: fundamentals to applications*. Cambridge University Press.

39. Thompson, A. P., Aktulga, H. M., Berger, R., Bolintineanu, D. S., Brown, W. M., Crozier, P. S., ... & Plimpton, S. J. (2022). LAMMPS-a flexible simulation tool for particle-based materials modeling at the atomic, meso, and continuum scales. *Computer Physics Communications*, *271*, 108171.

40. Stukowski, A. (2009). Visualization and analysis of atomistic simulation data with OVITO–the Open Visualization Tool. *Modelling and simulation in materials science and engineering*, *18*(1), 015012.

41. Stukowski, A., & Albe, K. (2010). Extracting dislocations and non-dislocation crystal defects from atomistic simulation data. *Modelling and Simulation in Materials Science and Engineering*, *18*(8), 085001.

42. Stukowski, A., Bulatov, V. V., & Arsenlis, A. (2012). Automated identification and indexing of dislocations in crystal interfaces. *Modelling and Simulation in Materials Science and Engineering*, *20*(8), 085007.

43. Plimpton, S. (1995). Fast parallel algorithms for short-range molecular dynamics. *Journal of computational physics*, *117*(1), 1-19.

44. Rowlinson*, J. S. (2005). The Maxwell–Boltzmann distribution. *Molecular Physics*, *103*(21-23), 2821-2828.

45. Williams, P. L., Mishin, Y., & Hamilton, J. C. (2006). An embedded-atom potential for the Cu–Ag system. *Modelling and Simulation in Materials Science and Engineering*, *14*(5), 817.

Appendix

Appendix A: Code for LAMMPS

A code for simulating tensile test of Cu-Ag core-shell nanowire of 40 Å core diameter and 10 Å shell thickness for a strain rate of 2 Å/ps at 25 K is presented below.

```
# MD Siulation of Cu-Ag Core-Shell Nanowire

#------------------------------- 1. Initialization
-------------------------------#

echo screen
dimension 3
boundary p p p
units metal
atom_style atomic

#------------------------------- 2. Structure Generation
-------------------------------#

lattice fcc 4.085
region silver cylinder z 0.0 0.0 30.0 0.0 200 units box
create_box 2 silver
create_atoms 1 region silver units box

lattice fcc 3.615
region copper cylinder z 0.0 0.0 20.0 0.0 200 units box

group core region copper
group shell subtract all core

set group core type 2
set group shell type 1

group Lower id < 5496
group Upper id > 27481
group Middle id <> 5495 27482
```

```
#-------------------------------- 3. Interatomic Potential
--------------------------------#

pair_style eam/alloy
pair_coeff * * CuAg.eam.alloy Ag Cu

#-------------------------------- 4.Equilibration
-------------------------------#

velocity all create 25.0 12345 rot yes dist gaussian units box
fix 1 all npt temp 25.0 25.0 0.01 iso 0.0 0.0 0.5

thermo 10
thermo_style custom step pe ke etotal temp lx ly lz press atoms

dump 1 all cfg 1000 CuAg_25.*.cfg mass type xs ys zs
dump_modify 1 element Ag Cu
dump 2 all custom 10000 dump.CuAg id x y z
log log.equilibration_25

timestep 0.001

run 50000

#-------------------------------- 5. Deformation
-------------------------------#

fix 2 Lower move linear 0.0 0.0 0.0 units box
fix 3 Upper move linear 0.0 0.0 2.0 units box

compute force Lower reduce sum fz
compute displacement Upper com
compute temperature Middle temp

thermo 10
thermo_style custom step c_displacement[3] c_force c_temperature

dump 3 all cfg 1000 CuAg_25.*.cfg mass type xs ys zs
dump_modify 3 element Ag Cu
dump 4 all custom 10000 dump.CuAg id x y z
```

```
log log.deformation_25

timestep 0.001

run 150000

#####
```